Universitat de Girona
Escola Politècnica Superior

Incoming Exchange Student - Master Thesis

Erasmus ■ Techno □ Other (specify):

Title of master course: Master in Enginyeria Industrial

Title of master thesis: Implementation of fracture test of concrete to determine fracture properties

Document: Master Thesis

Student (Name & Surname)**:** Bram Plancke

EPS Advisor: Dra. Cristina Barris
Department: Arquitectura i Enginyeria de la Construcció

Delivered on (month/year): 06/2015

KU LEUVEN

FACULTEIT INDUSTRIELE INGENIEURSWETENSCHAPPEN

TECHNOLOGIECAMPUS GENT

Implementation of fracture test of concrete to determine fracture properties

Bram PLANCKE

Promotor: Dra. Cristina Barris
Escola Politècnica Superior
Universitat de Girona

Masterproef ingediend tot het behalen van de graad van master of Science in de industriële wetenschappen bouwkunde, afstudeerrichting bouwkunde

Academiejaar 2014-2015

Universitat de Girona

Master Thesis

Implementation of fracture test of concrete to determine fracture properties

Màster en Enginyeria Industrial

Presentation date

18 June 2015

Author

Bram Plancke
Master MMS, EPS UdG
Bram.plancke@student.kuleuven.be

Adviser

Dra. Cristina Barris Peña
Enginyeria Mecànica i De la Construcció Industrial, EPS UdG
Cristina.barris@udg.edu

ERASMUS+ student at
Escola Politècnica Superior - Universitat de Girona
Campus Montilivi - 17071 Girona
http://www.udg.edu

Universitat de Girona

Home institution
Faculteit Industriële ingenieurswetenschappen - KU Leuven
Technologiecampus Gent - 9000 Gent
http://iiw.kuleuven.be

KU LEUVEN

Word of thanks

After an intensive period of 4 months, these are the last words of this thesis that are being written. During this period I have learned a lot, not solely scientifically or technically speaking, but also on a personal base.

This thesis is the result of a lot of research, collaboration, choices that had to be made, and planning. It would not have been possible to manage all of the aforementioned without the help of my adviser, Dra. Cristina Barris of the department of *Enginyeria Mecànica i De la Construcció Industrial,* Universitat de Girona. Thank you for the needed guiding and accompanying aid during the whole process.

I would also particularly like to thank my colleague-student, Xayvanh Oundala, who was doing research on the same matter, with whom close collaboration was very fruitful. Together with him and Dra. C. Barris, influential decisions regarding the tests and results in this thesis were made.

A well-meant thank you goes out to Pere Bellvehi of the *Dept. Arquitectura i Enginyeria de la Construcció* for helping us with the fabrication of the specimens in the Structures Lab of UdG, and to Sergi Saus of the Mechanical Lab for manufacturing a considerable part of the test setup.

Furthermore I would like to say thank you to Irene Villanova and the rest of the AMADE (*Analysis and Advanced Materials for Structural Design*) research group, who have made their lab and testing equipment available for us, and had a great share in the programming, calibration and teaching how to operate the test setup.

Thank you all!

Bram Plancke

Girona, 13th of June 2015.

Table of contents

1 Introduction

This master thesis aims at implementing a three-point-bending test for concrete where the fracture energy can be deduced. The test will also try to record the softening curve of concrete after cracking. The Digital Image Correlation (DIC) technique will also be applied, for the most interesting case, in order to determine the strain field along the test. For this purpose, test procedures have to be studied along with acquiring detailed knowledge on the fracture energy G_F. Multiple tests will be performed to assess data and to interpret results, so conclusions could be formed.

The main goal of this thesis is carrying out a three-point-bending test for concrete where the fracture energy can be derived. Therefore, a state-of-the-art review concerning fracture mechanics of concrete is first needed. Correct results for the fracture energy and bilinear softening curve of concrete are what are aimed for. Although the AMADE research group has precious experience in fracture mechanics of composite materials, it was the first time this test was performed for concrete at the UdG. Like all research where little in that specific field is known, a lot can go wrong. Failure of tests, incorrect or unusable data, adaptations to test setups, unclear instructions… Solutions to all those complications must be found before reaching correct results. Whenever it is clear *why* these correct results cannot be obtained, and a probable solution to the problem can be presented, and using/analysing the DIC (Digital Image Correlation) technique is comprehended, the goal of this thesis is reached.

2 Structure of this thesis

In the following chapter, a state-of-the-art review about fracture mechanics of concrete and the digital image correlation technique is done. A deeper understanding of those topics is of utmost importance on the way to achieving aforementioned goal of this thesis. The most influential works per topic are summarized and cited in 3.1 & 3.2. In 3.3 the most meaningful guidelines are chosen and explained.

Chapter 4 describes all the complete experimental test setups of the three-point bend test and the DIC technique that were utilized. Machines used, instrumentation, machine settings, and materials are all clarified. Manufacturing and processing of the concrete specimens was done in the *Structures Lab of EPS*. The majority of tests took place in the AMADE lab in *Parc Científic i Tecnològic de la Universitat de Girona*, whereas the analysis of test results and DIC study took place in the *Escola Politècnica Superior* buildings.

In chapter 5, the experimental test setup is applied. First, two trial tests are performed to become familiar with the test and solve all complications and unknown factors. After the trial tests, definitive specimens are tested. These definitive specimens consist of two differently composed sets of four concrete beams (4 x C30 and 4 x C50). The experimental results are then analysed, compared and discussed. An evolution of adaptations (machine settings, specimens geometry…) for ensuing tests considering previously gathered results is also specified.

The determination of modal parameters such as the initial portion of the cohesive crack model, fracture energy and the bilinear softening curve are found in chapter 6. Used formulas and calculations leading to results are analysed so conclusions could be formed.

Chapter 7 includes general conclusions about this thesis, with propositions for future tests.

3 State-of-the-art review

This section includes previous works about fracture mechanics of concrete and DIC which were studied, as well as which and why some were chosen as a guideline.

Since little is known about (tests related to) fracture energy of concrete in *Universitat de Girona*, an example study with results to pursue would make it easier to come to conclusions with respect to aforementioned goals. Not only the concrete type and properties (largest aggregate size, W/C-factor, cement type...) were of importance, but also the specimen size, notch width and depth, and curing method. Further questions were how the test setup and settings had to be, what parameters were interesting to change, if the size effect [1]–[3] was applicable, what is measureable, speed ratio of the displacement, what peak load to expect on the specimens etc.

3.1 Fracture mechanics of concrete

The relevance of the tensile fracture behaviour of quasi-brittle materials for structural design is well established and can be quantified by means of the fracture energy G_F [4]. This parameter is useful for design purposes, as pointed out in several examples [5], as well as for modelling the fracture behaviour of cohesive materials, as reported in some recent reviews [6]–[8]. The application of concrete fracture mechanics is found in a wide area of toughening mechanisms like in fibre-reinforced concrete, fatigue fracture of concrete, and the effect of creep on concrete crack growth and fracture [9].

Fracture process is a fundamental phenomenon in concrete materials. The fracture energy is defined as the amount of energy necessary to create one unit area of a crack. Different methods are found in the literature to determine some fracture parameters such as the fracture energy (G_F) of concrete by means of three-point bending tests on notched beams [3], [10], [11]. The question of a proper fracture test standard for concrete and other quasi-brittle materials like cementitious materials has been intensely debated since the 1980's (e.g., Bažant and Planas, 1997) [2]. A basic and necessary ingredient of cohesive crack models, so widely used for numerical quasi-brittle fracture simulations, is the softening function which characterizes the property of concrete-like materials [10]. In this thesis this (bilinear) softening curve with the initial and total fracture energies is one of the wanted results.

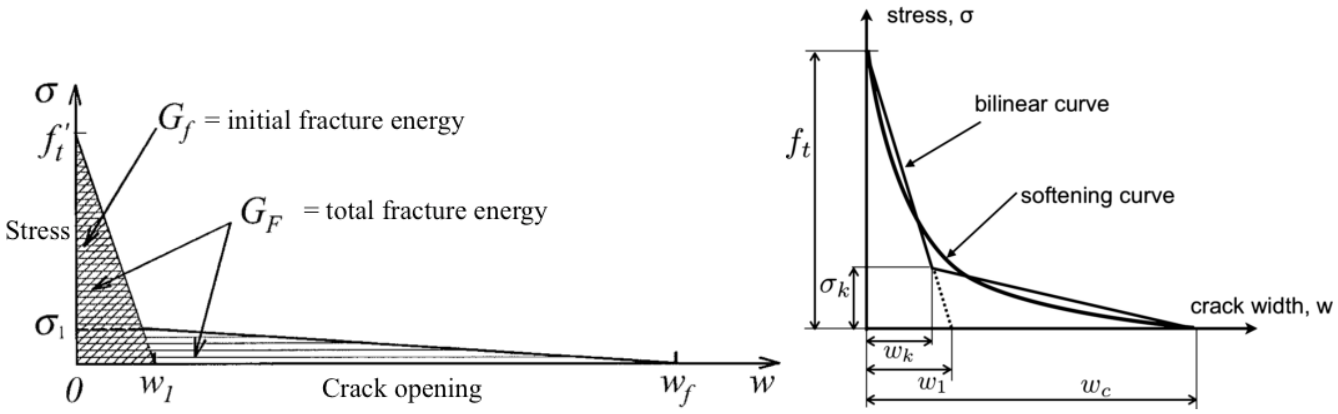

Fig 3-1 - Bilinear softening curves of cohesive crack model for concrete

3.2 Digital Image Correlation (DIC)

In the field of experimental mechanics optical full-field measurement methods such as Digital Image Correlation (DIC) are more and more used. They are very promising tools for the experimental analysis of the mechanical properties of materials and structures. The main techniques are photoelasticity, moiré, holographic and speckle interferometry, grid method and digital image correlation (DIC) [12]. In the context of this thesis, it will be the DIC technique that is used. DIC has been found to be a flexible and effective technique to measure the displacements on a specimen's surface by matching the reference subsets (i.e. black speckles on a white background) in the undeformed image with the target subsets in the deformed image [13]. Easily put, points are tracked on each taken photo so that the displacements and relations between those points over multiple photographs are known.

Conventionally, the responses of structures under external load are measured with wired sensors directly attached to the structures. Linear variable differential transformers (LVDTs), or HLS's in the case of this thesis, and strain gauges are typically used to measure displacements and strains. The disadvantage of this method is that only one local measurement is made at the time [14]. For large structure tests this may require much labour from professional technicians, a lot of cabling and instruments. Also the maintenance and needed calibration of the sensing systems can be time-consuming and costly. Thanks to the rapid development of image acquisition systems and better computational algorithms, contactless measurements such as the DIC technique have thus gained increasing acceptance in experimental mechanics. The DIC technique has for example already been applied to observe dynamic characteristics of several structures [15][16].

3.3 Main guidelines

ACI 446 (with test Type II in mind) was chosen for the test procedure, since it has the most detailed steps to follow. It will later become clear the test method was rather Type I than Type II due to machine limitations. Regarding the calculations of the concrete properties based on test results, an easy-to-follow summary [17] based on ACI 446 was used. This same paper was also a good guidance for the choice of concrete composition and specimen dimensions. RILEM's 50-FMC was an option for the test procedure as well, but seemed incomplete and unclear at some points, due to it being quite obsolete.

As for the DIC-technique, knowledge and help of AMADE members were at hand, as well as their manual [18].

4 Experimental test setup

The guidelines for the bending test setup of ACI 446 were mainly followed, as well as some parts of an *improved version of the method proposed to ACI 446 and to RILEM TC 187-SOC* [17].

For the DIC-setup, the AMADE guideline [18] was followed.

4.1 Three-point-bending test

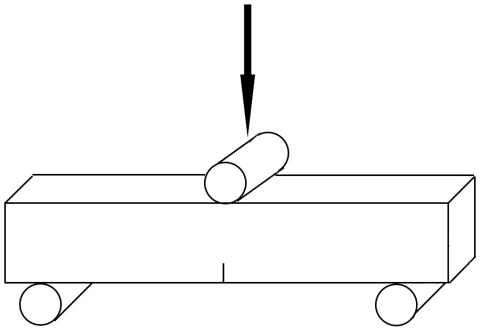

Fig 4-1 - Three-point bending test representation

To determine the fracture energy of concrete, the three-point bending test measuring the maximum loads of geometrically similar notched concrete specimens, is recommended for the purpose of standardization. The beam, of length *L*, rests on two roller supports and is subject to a concentrated load P at mid-span [1]. This way, the load versus crack mouth opening displacement (CMOD) can be measured to help determine the fracture characteristics.

4.1.1 Setup

The *MTS Insight® Electromechanical Testing System - 100kN Standard length* apparatus was used for the three-point bending tests of the trial specimens and all C30 specimens. ACI 446 proposes following setup for the placement and support of the specimen in the machine [19]:

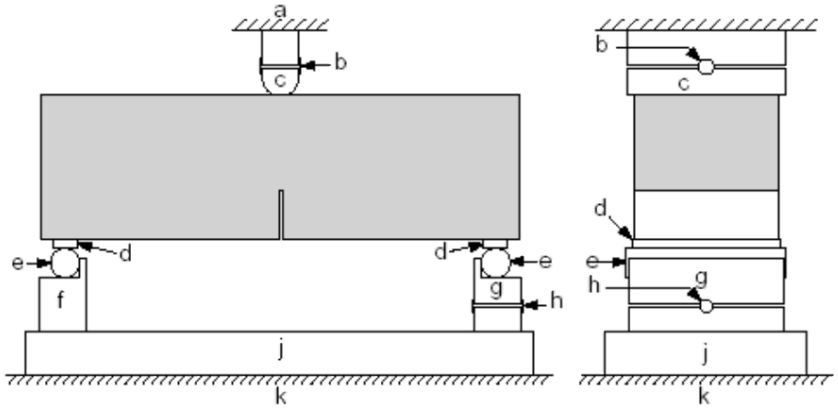

Sketch of the loading apparatus: (a) load cell; (b) hardened steel shaft; (c) rotating loading block; (d) hardened steel bearing plates; (e) hardened steel rollers; (f) fixed support; (g) rotating support; (h) hardened steel shaft; (j) stiff steel beam; (k) machine frame.

Fig 4-2 - Representation of the loading apparatus proposed by ACI 446

In order to make the specimen fit the apparatus like above figure, a custom steel support beam was designed and manufactured by UdG's mechanical lab. This support consists of a steel I-profiled beam as a base, with parts of the same profile to form the specimens roller supports bases on top of it. At the extremities of the rolling surfaces, small steel bars were welded as precautionary rolling limiters.

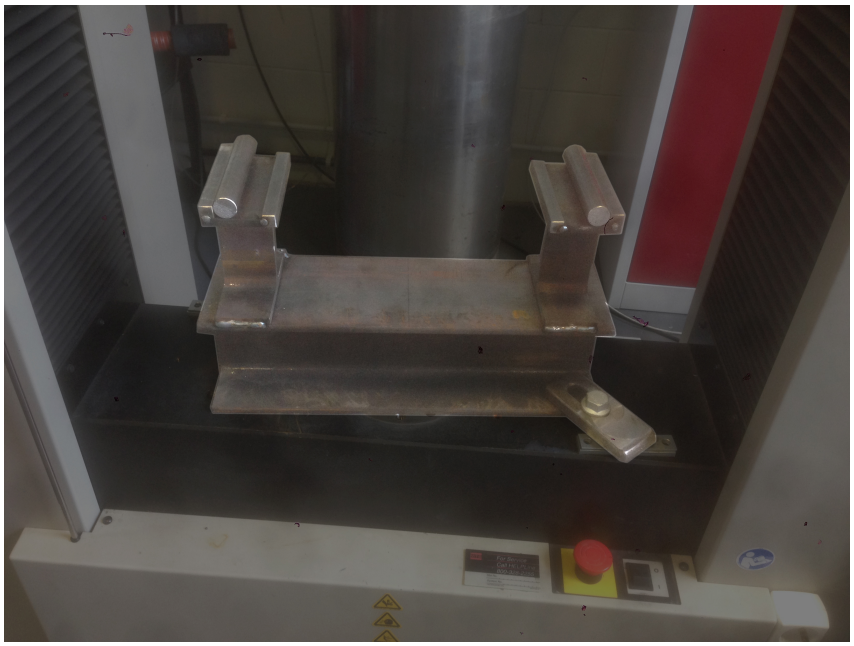

Fig 4-3 - Custom specimen support beam and rollers

4.1.2 Instrumentation

4.1.2.1 Load point displacement (LPD)

To measure the vertical displacement of the load point in the top centre of the beam, without the inelastic deformation associated with the supports, a reference frame resting directly above said supports was needed.

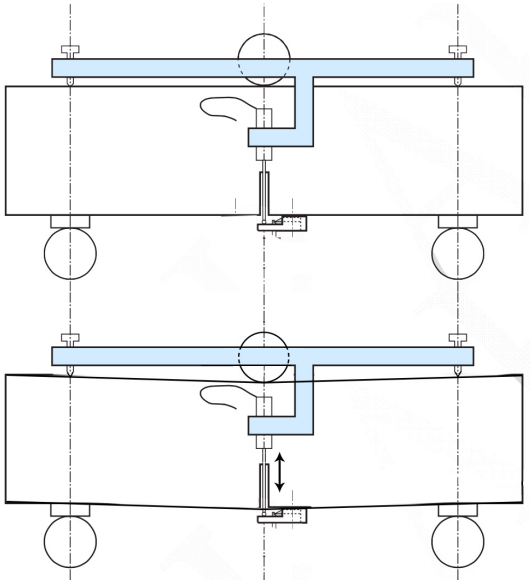

Fig 4-4 - Reference frame intention

Attached to this frame are two HLS sensors (*Modelo LDS HS-100.- Sensor de desplazamiento extensométrico. (Linear Displacement Sensor)*), one on each side, to measure the vertical displacement. Two aluminium plates are glued to the centre bottom of the beam on each side, by means of a resting (reference) point for these HLS's. This frame (see Appendix A – Reference frame) was designed during this master thesis to fit the specimen's geometry and hold the given HLS's.

The result was the following:

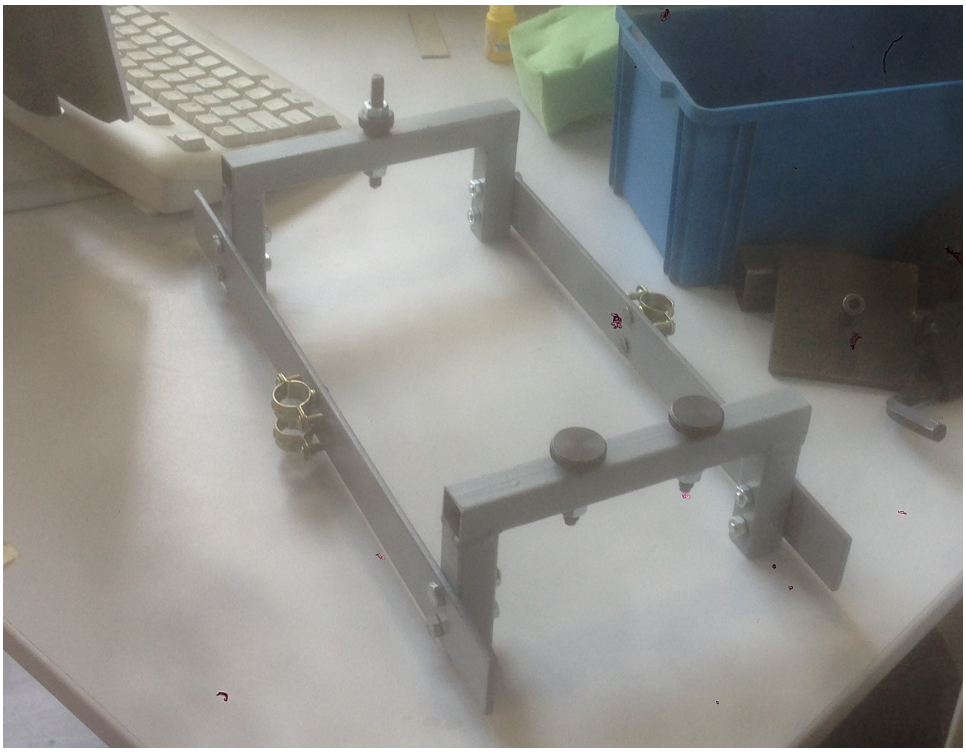

Fig 4-5 - Built reference frame with 2 HLS holders per HLS to limit rotation

4.1.2.2 Crack mouth opening displacement (CMOD)

One of the more interesting data to collect during testing is the crack mouth opening displacement (CMOD). This is easily done using a clip gauge extensometer, attached between two knives placed across each other, in the middle of the notch length. Some requirements in ACI 446 are put together in a drawn representation:

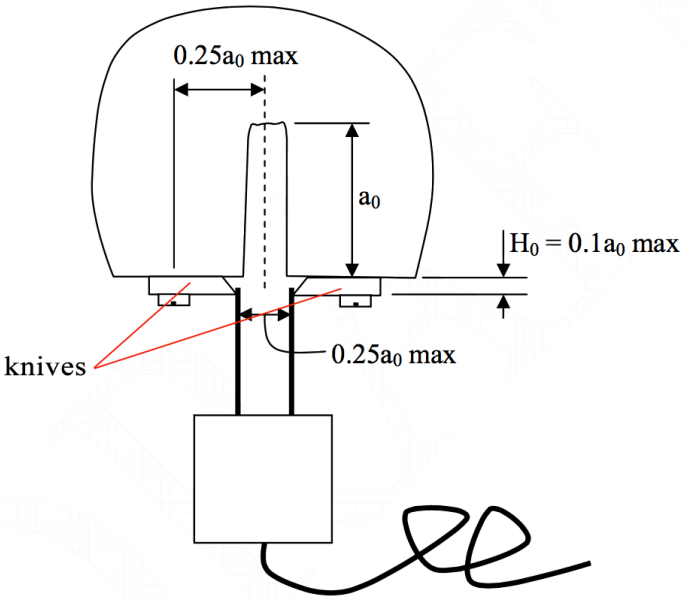

Fig 4-6 - Detail of the extensometer placement and distances to respect [19]

The used extensometer (*Epsilon Technology Corp model 3541-005M-120M-ST*) had a minimum opening of 5 mm. The maximum opening is $0{,}25.a_0$ = 8,25 mm (with a_0 being 33 mm), so this requirement was met. Regarding the knives, the thickness was also smaller than the maximum value. Fixation of the knives was not done via screws but was glued, to make sure the specimens did not get damaged in the attaching process.

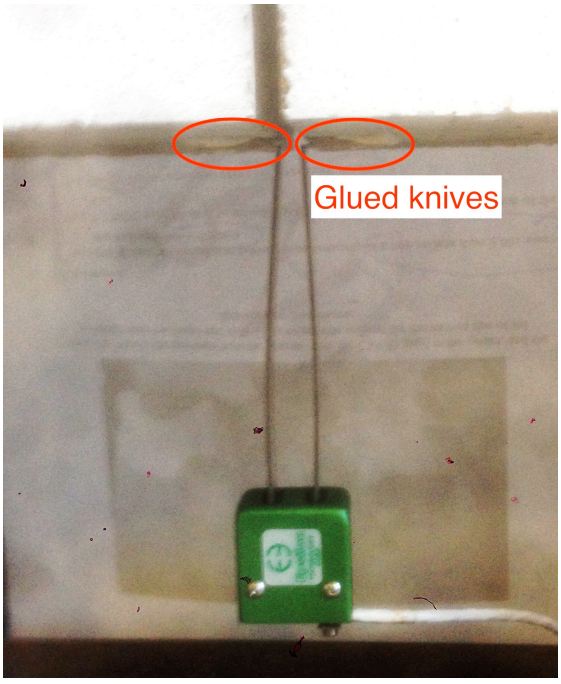

Fig 4-7 - Extensometer held by 2 knives at the notch opening

4.1.3 Total 3PBT setup

In Fig 4-8 the placement of the reference frame with HLS's is shown. Fig 4-9 is a photograph of the total setup taken right before testing the first trial specimen.

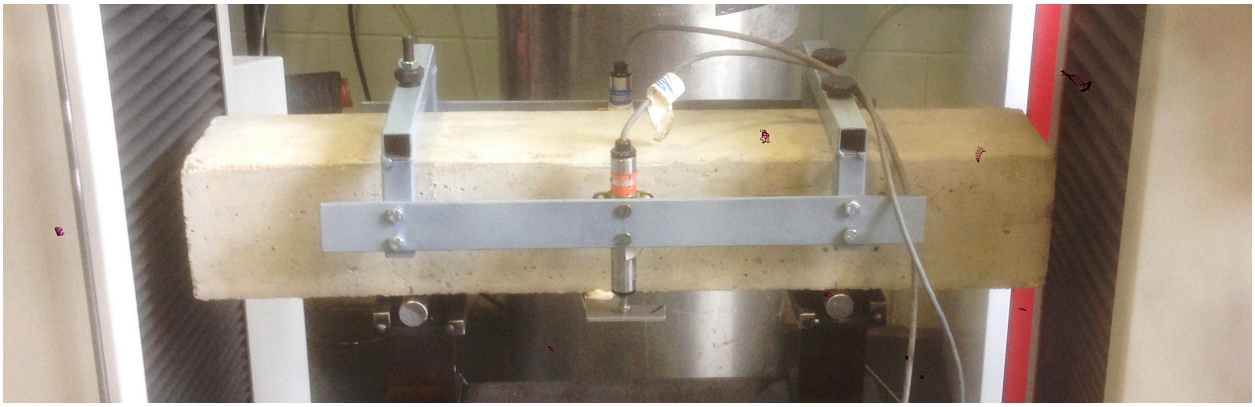

Fig 4-8 - Specimen with reference frame with mounted HLS's

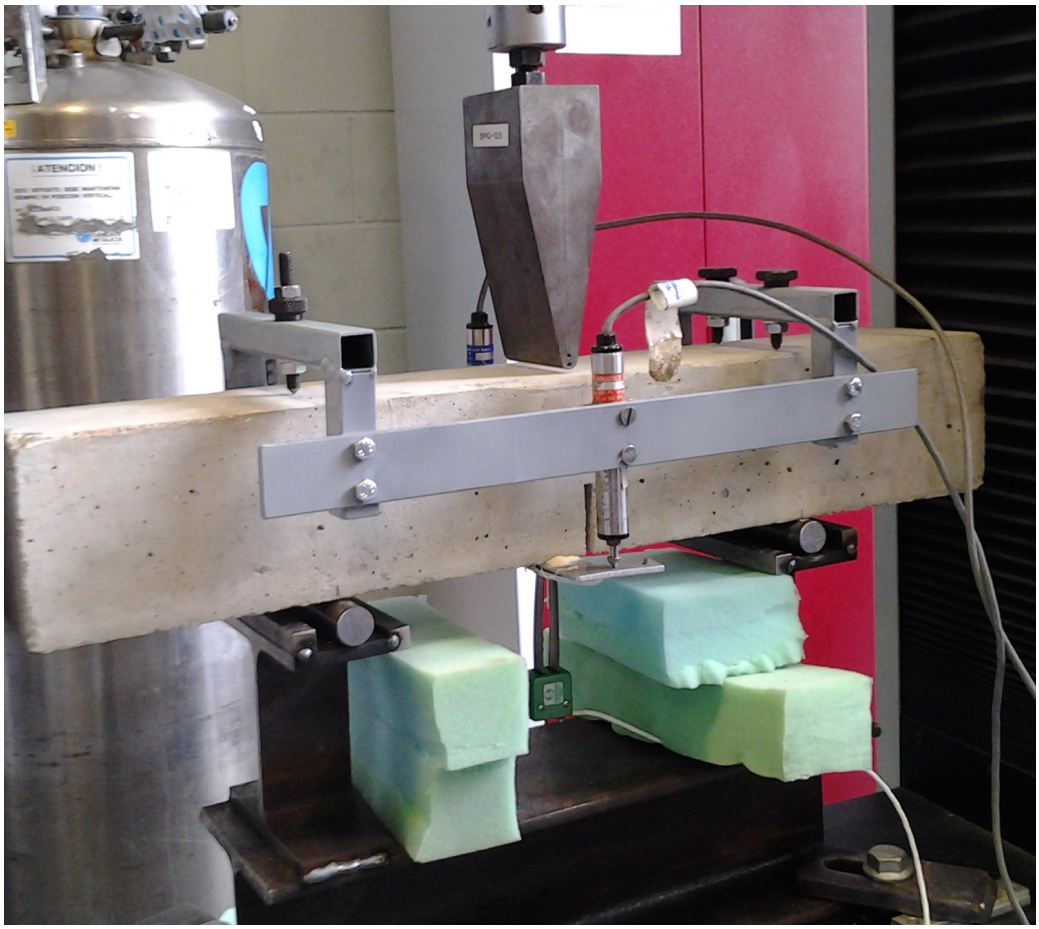

Fig 4-9 - Photo of the complete setup (NOTE: incorrect loading block (see 4.1.5) and protective foam for if the beam would snap in two)

4.1.4 Machine settings

For the fracture mechanics test, a sufficiently stiff servo-hydraulic or electromechanical testing machine with closed-loop control with the crack mouth opening displacement (CMOD) as the feedback signal is preferred rather than without closed-loop servo control [1], [19]–[21]. Slight adaptations had to be made since no CMOD feedback signal was possible with available testing machines. Instead, the load point displacement (LPD) had to be used with manual displacement speed input. For that reason, before testing the real specimens, two trial tests with similar specimens were done (see paragraph 5.1). Because the 2 trial specimens were the first to ever be tested by a three-point bending test, a lot of information was unknown. For example the estimated peak load (to determine the pre-load) and the load point displacement (LPD) speed.

4.1.4.1 Load point displacement speed

For the first trial test, 0.06mm/min (0.001mm/s) was used as the vertical displacement speed. The peak load has to be reached within a time interval of 3 to 5 minutes. [19], This was not the case for the first trial test, so for the second trial test the speed had to be increased. As could be calculated from the results of the first trial, the displacement rate was more or less doubled to 0.1mm/min for the second trial, to reach the peak load sooner (see 5.1.1). After analysing the trial test results, relationships between LPD & CMOD and CMOD & peak load could be found, which was important to determine the load point displacement speed for the definitive specimens to reach the peak load within 3 to 5 minutes [19].

4.1.4.2 Data registration

Registering data is recommended at 0.1s intervals [19], but in our case data was registered at 50Hz, meaning every 0.02s. This was to make sure enough data was collected. Afterwards, taking the average of every 20 values for example could easily decrease the total registered values.

4.1.4.3 Pre-load

Cited from ACI 446: *"…and slowly pre-load the specimen up to a load of between 5 and 10 % of the estimated maximum load. After the test, this pre-load shall be checked not to have exceeded 15% of the actual peak load. If this limit has been exceeded, the test shall be considered invalid.* [19]*"*

Contrary to reinforced concrete, there are no obvious formulas to estimate the peak load of a beam with given dimensions. Therefore, it came in handy we had used similar beams and concrete type to previously found papers [17]. In an improved version of ACI 446 [17], where values are added to the theory, they use beams of similar size and analogous concrete strength for the (assumed) C25 specimens (these were actually ≈C18, see 4.3.6 Compressive strength):

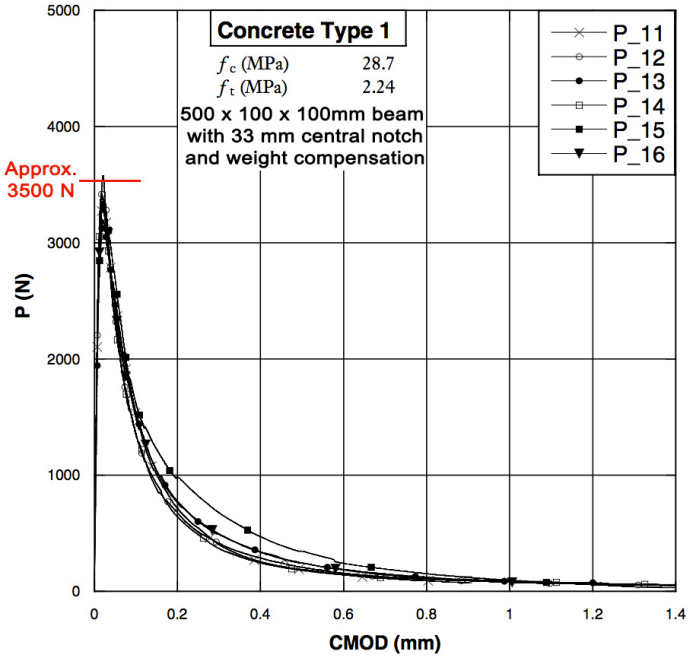

Fig 4-10 – Load – CMOD curves for multiple C30 specimens [17]

As can be seen on above figure, the peak load for similarly sized C30 specimens was around 3,5 kN. As a pre-load for the trial specimens we chose to use 5% of this peak load to make sure this pre-load would not exceed 15% of the real occurring peak load. For each following test, the pre-load was either based on a previous test of the same concrete type, or guessed based on another paper's results [17].

4.1.4.4 End of the test

"*The test may be terminated after CMOD exceeds 4D/300.*" [19] In our case, with D = 100 mm, this meant stopping test whenever the crack mouth opening displacement reached a total of 1,33 mm. The test should also be completed within 30 minutes [19], but this was ignored since the speed of the test could not be adapted without restarting it.

4.1.5 Setup adaptations

- In the previous paragraph it is stated that no machine was available with CMOD control, which is why a (constant) displacement speed was opted for.
- For the first trial test, an incorrect loading block (too short and diameter too small) was used because the correct one, *cylindrical with a circular boundary of a radius 0.1 D* $\leq$ *R* $\leq$ *0.2 D and a length equal or exceeding the specimen width* [19], was not ready yet. This lead to a more concentrated load in the centre of the beam, rather than a linear load along the whole depth of the beam. This has also affected the displacement registration of the HLS sensors (see 5.1.3). The difference between loading blocks can seen on the picture below:

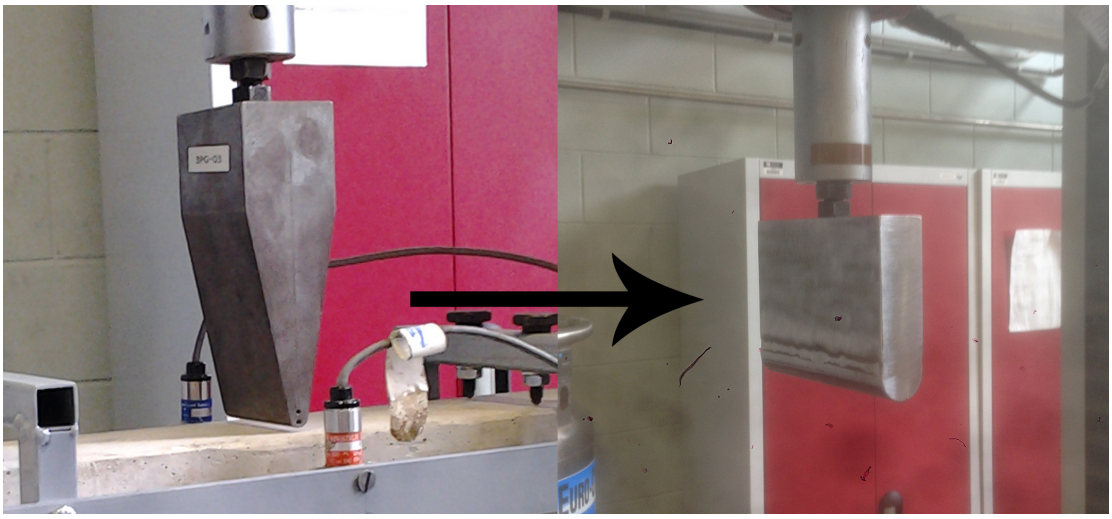

Fig 4-11 - Difference between 2 loading blocks

- Another adaptation was not using the roller support plates, since they could not easily be reused after testing because of the glue and sticking concrete debris not being totally removable. A flat surface for total contact between roller and concrete was instead guaranteed by sandpapering the concrete, and whenever needed, putting small metal spacers in between.

4.2 Digital image correlation (DIC) technique

DIC is a recently used contactless technique that has a lot of advantages. It measures fields of displacements and deformations of specimens of choice. Two different configurations for digital image correlation exist: 3D and 2D, these are discussed in 4.2.2.

The main goal of the DIC technique implementation in our case was measuring the crack opening displacement, as well the load-point displacement and strains in proximity of the crack to determine stresses. The actual width of the crack was measured so it could be compared with the measured COD by the extensometer to form a conclusion.

DIC can have a lot of advantages. In the case multiple very small displacements are wanted, the digital image correlation technique can be easier to use than a dozen measuring devices. Apart from the DIC setup itself at a distance, the specimen stays 'wireless', this means the work area is less cluttered and focussing on the specimen is easy. DIC also has the great advantage of being able to make new measurements (i.e. between different points) after testing. For small specimens the calculated strains in a whole area of interest can easily be retrieved.

When using the DIC technique at UdG, the programmes *VICSNAP*, *VIC-3D* and *VIC-2D* (licensed software) come at hand. Although they are fairly easy to use, these programmes have their flaws. One, for example, is the calibration of the 3D setup. This calibration can work at the first trial, but may also be very hard to achieve, even if the surroundings remain the same. This can make it interesting to switch to a (sometimes less accurate [22]) 2D-test. Other problems occur when trying to collect measured data. This will be discussed later on (see 4.2.1.1 Flaws).

Before elaborating about those flaws, the setup must be reminded: the machine for the 3-point-bending test (3PBT) registers load point displacement (LPD), time, crack mouth opening displacement (CMOD) and load. To make it possible to synchronize DIC data registration with 3PBT data, a connection is made between the two setups. The data registration is then manually started at the "same" time. Only one connection between 2 setups was possible, so the only shared variable was the load. A simplified representation of this connection and registered data is sketched below:

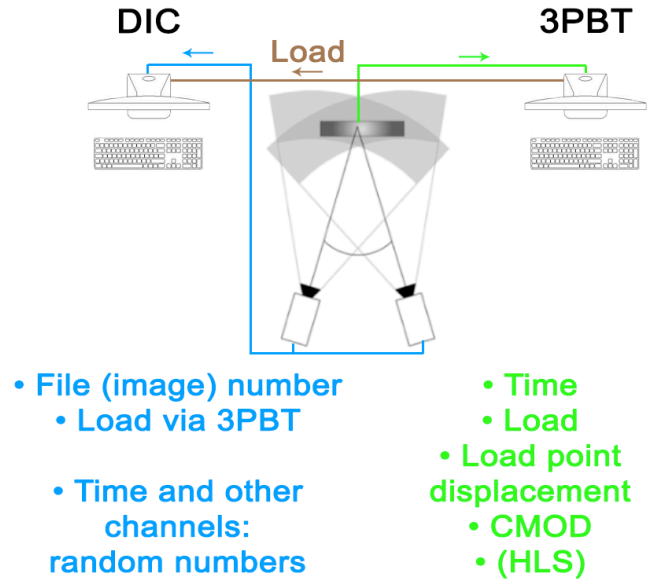

Fig 4-12 - Simplified representation of the 3PBT & DIC setup conjunction

Since time is not registered on the DIC-setup (in our case, this can be different!), it is harder to synchronize the data when processing it. For DIC the time-axis actually is an "image count"-axis. So to compare graphs (for example CMOD over time), x-axis' need to be scaled equally. This is the tricky part: the frequencies of registration of both setups (DIC: images/second, 3PBT: values/second) need to be known and compared.

For example: DIC registers at 2 images/s (= 1 value every ½ second), and 3PBT registers at 50Hz (1 value every 0,02 seconds). The solution was taking the average of every *n* 3PBT values until they were equivalent to 1 value every ½ seconds. For this purpose a MATLAB code was written for Mac -but adjustable to Windows, shown in `REMARK1`- (see Appendix B – MATLAB average code).

An attentive reader will quickly remark this of course only works if the registration frequency of both setups stays the same. If for some reason, during the testing, the DIC photographing rate is changed, above MATLAB code needs to be ran 2 or more times, with the starting point of the new frequency manually searched for. This was the case for the C30_4 specimen, shown later. This is a lot of work and therefore it is preferable to not change any DIC or 3PBT setup settings during testing. If this is not possible, data will have to be treated before analysis.

4.2.1.1 Flaws

As stated in 4.2 there are some flaws when using the DIC technique.

A first flaw in the programmes needed for the DIC technique, is when analysing the results. Dots can be placed anywhere in the selected surface on the beam, and all info like displacement in x, y (and z in 3D) and strains in that point can be collected. When closing the programme and re-opening it, the dots are not remembered. This gives complications when working on the same test results over a diffused period of time and new dots have to be extracted with the placement of previous dots in mind. Screenshots were taken to remember the place of each dot.

In the same line as the previous flaw, there is no on-screen grid available in the programmes. When comparing data for different specimens, it would be very interesting to place dots at the same coordinates, which is impossible without grid and on-screen ruler. Literally placing a ruler on a computer monitor is not accurate to say the least. This could easily have been prevented though if the specimens were marked before being tested, but we were unaware this would have been an issue.

Also the calculated strains do not seem to be correct for large specimens (like in our case). See the results in paragraph 5.1.7 for examples.

4.2.2 DIC setup

Two methods of using DIC are possible, 3D and 2D. As stated above, 3D results are more accurate, but the setup is harder to calibrate. Two-dimensional DIC practically always calibrates from the first try, but cannot measure out-of-plane deformations. This derives in less accurate results [22]. The used cameras were AVT Stingrays.

4.2.2.1 The 3D setup

The 3D setup uses 2 cameras for the same field of view (FOV), which capture a photo at the same time. Both images are then put together into 1. To get a 3D image (with depth), it is important to get the right angle between 2 cameras. This angle depends on distance to the specimen, and type of focal length of the lens. Choice of lens is mainly depended on the field of view (FOV) and its diaphragm; how much light is available in the room?

As shown in the DIC-setup manual of AMADE [18]:

"Once a lens and approximate distance is selected, the cameras can be pointed. The cameras should be positioned somewhat symmetrically about the specimen; this will keep the magnification level consistent. The exact angle included between the cameras is not critical but selecting a correct stereo angle will give best results":

Available devices	Focal length [mm]	Stereo angle α [º]	Field of view [mm]
4	8	25	200 to 10000
4	23	20 to 25	100 to 250
2	60	10 to 20	25 to 200
2	120	10 to 20	3 to 8

Table 4-1 - Possible angles depending on focal length

The angle should be kept below approximately 60º.

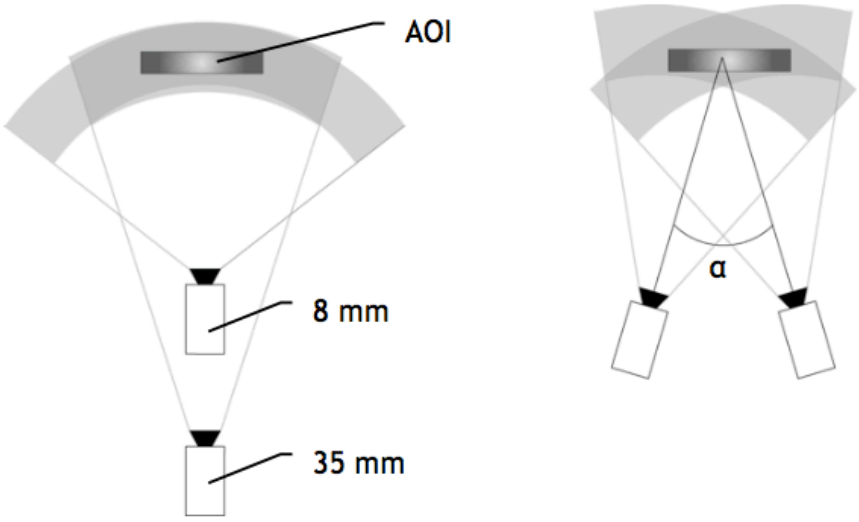

Fig 4-13 - Examples of camera positions depending on AOI = Area of interest

In our case the used lenses were 1.4/8mm Schneider Cinegon. The cameras were placed at a central distance of 370 mm to the specimen, with an angle of 20° between both cameras. This meant a distance of 130 mm between both cameras on the slider.

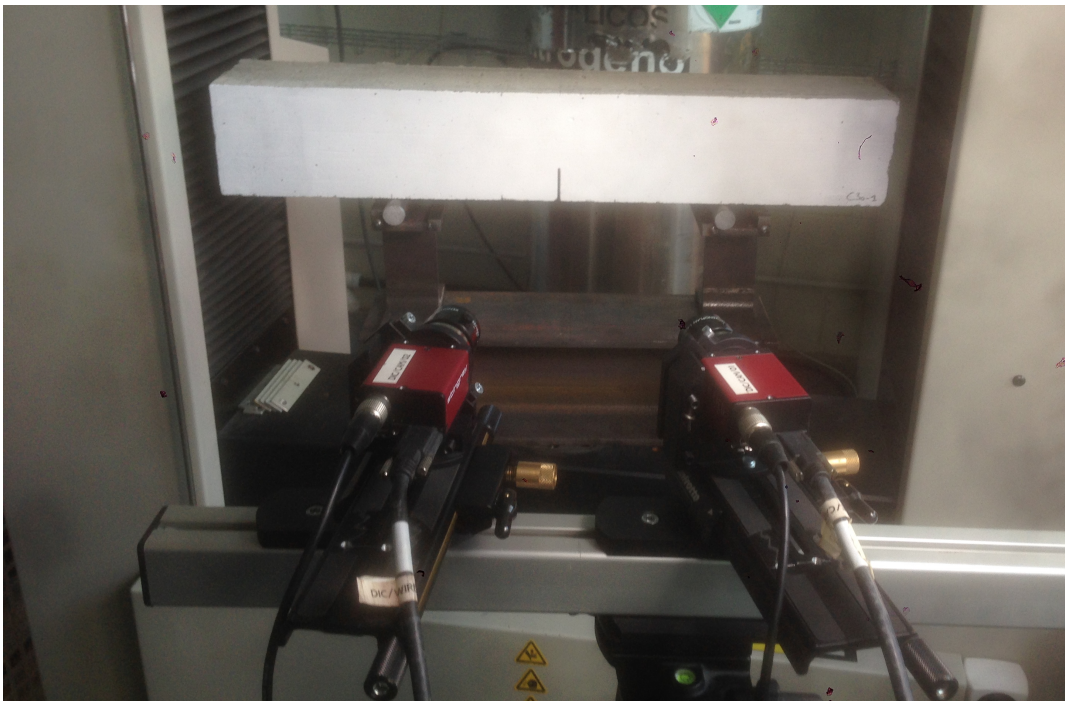

Fig 4-14 – 3D setup with lighted beam in the background

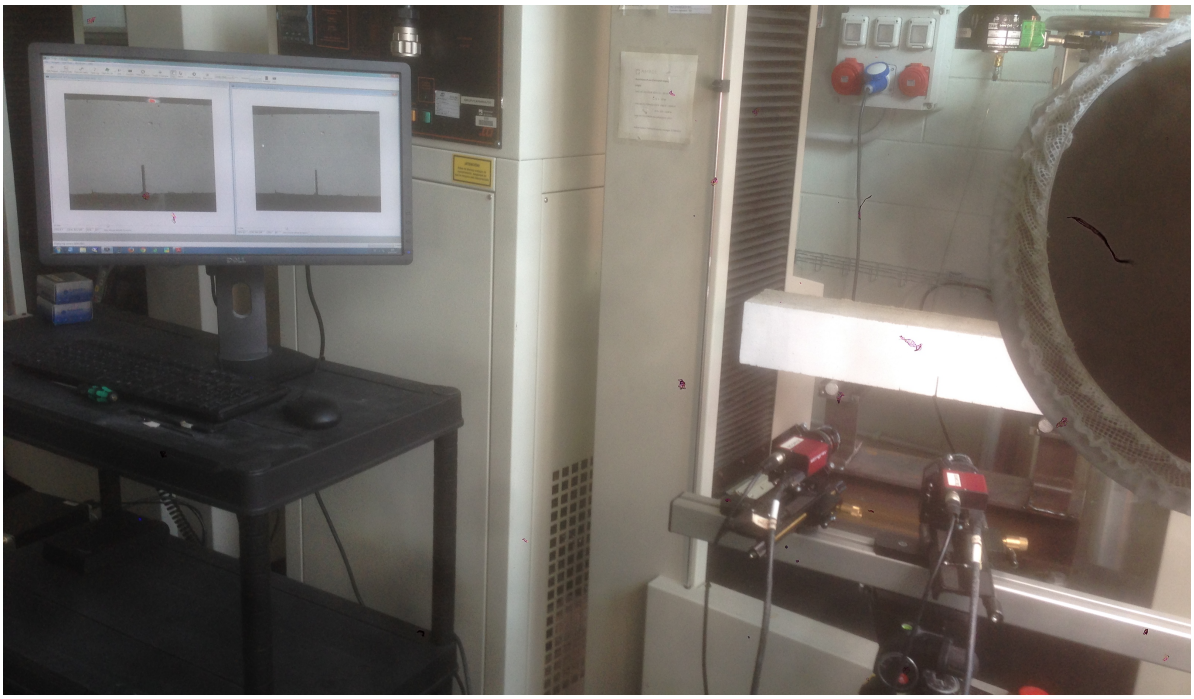

Fig 4-15 – The live on-screen images of both cameras help placing and focussing them

4.2.2.2 The 2D setup

The main difference between 3D and 2D regarding the setup is that only one instead of two cameras is used (no photo was taken of this setup). One of both AVT Stingray cameras is set up to point the middle of the specimen perpendicularly. The distance to the area of interest remains roughly the same, as the tripod and slider supporting the camera stays in place, only the angle changes, since the camera has to point the AOI perfectly perpendicularly.

4.2.3 Speckle size

To determine all deformations and displacements, the DIC technique follows the movement of and relationship between different black speckles. These black speckles are applied on the white surface by spraying them using an airbrush. The optimal size depends on a lot of factors; larger speckles means there is a sufficiently distinctive intensity pattern contained in the subset to distinguish itself from other subsets, whereas small speckles guarantee a reliable displacement measurement [13], [23]. A speckle's diameter should be around 4-6 pixels. Trials are sprayed on white paper first and then held in front of the camera(s) at the same distance as the area of interest. If the speckles are small and numerous, and still sharp and discernable when zoomed in, they are good to use. The specimens can then all be sprayed in the area that interests us the most, the field of view or area of interest: a square of 10 x 10 cm around the central notch.

4.2.4 Calibration

Calibration is an important step when using the DIC technique, because the programme needs to recognise the speckles properly in order to have accurate results. The 3D stereo calibration process is quite easy to perform, but as stated earlier, this does not mean it will always work. The process consists of choosing a panel with a certain amount of black dots with a specific size, and on which three dots have a white inner dot. After taking about 40+ images of this grid in a different position, the programme will track all the dots (and this is why the 3 white dots are important for the calibration), after selecting which board was used (size of dots).

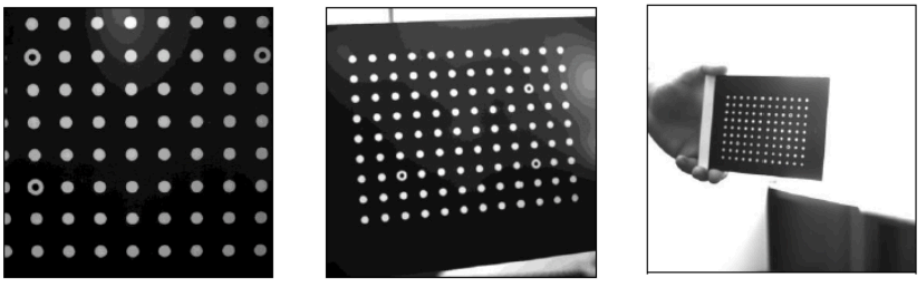

Fig 4-16 - Example of a calibration panel [18]. Left, too large – centre, correct grid – right, too small

For the 2D calibration, the image should only contain a real distance, for example between two points, which is given as input in the programme. It must be ensured that the length specified in the calibration is larger than half the length of the image diagonal. The software is then capable of converting pixel movements into physical displacements.

4.2.5 Settings

Once the setup is ready and calibrated, and the lenses are focused, the test could start. The only setting that was changed for different tests apart from using 3D or 2D was the frame rate. Depending on the duration of a test, different image registration frame rates were more justified. They varied from two images per second (relatively fast load rate) to one image every two seconds. Always make sure enough images are captured to acquire enough data-points over time.

4.3 Materials

Two trial specimens (labelled Trial_C18_1 and Trial_C18_2) without specific compositions in mind were cast before the definitive ones. It must be said these specimens were cast with a lot of uncertainties; decisions about geometry and notch for example were made based on the collective knowledge through research, but long before a clear guide to follow or to compare to was known. Timing was important since concrete needs 30 days to harden, and results of these trials were needed as soon as possible to move on to the definitive specimens. Only two moulds were available at the time, which is why only two trial beams (and accompanying cylinders for compressive tests) were made.

As for the definitive specimens, four beams of each concrete type were made in wooden moulds. These specimens were named C30_1 to C30_4 and C50_1 to C50_4. In addition to these beams, two standard cylindrical specimens 150 mm in diameter and 300 mm in length of each concrete type were made together with 1 standard cube of 200 x 200 mm. These were used to obtain the concrete properties. Both concrete types were made in one batch, and they were both cast on the same day. The reason why not three, but two cylinders plus a cube (smaller volume than a cylinder) were made is because the concrete mixer could not hold a larger concrete volume.

4.3.1 Specimen properties

Trial specimens	≈ C18	Remarks
W/C	0,60	
Cement I **32,5R**	15%	
Water	60%	Of cement mass
NCA 5/10	40%	
NFA 0/2	35%	

Table 4-2 - Composition of the trial specimens

The composition of the concrete types was a point of discussion before having a clear goal in mind, as stated in the State-of-the-art review. Would changing the maximum aggregate size be interesting? Or the water/cement factor [24]? Once the choice of following ACI 446 was made, the 'choice of parameters to change' was reduced to just using 2 different concrete types and see if the test was reliable and results as the softening curve could be deducted.

Two known compositions previously mixed by Universitat de Girona were used:

Definitive specimens	C30	C50	Remarks
Total needed volume [m^3]	0,04+10%	0,04+10%	4 beams, 2 cylinders, 1 cube + loss
W/C theoretical	0,60	0,42	
W/C when mixing	0,680	0,429	To obtain better viscosity
Cement I **52,5R** [kg/m^3]	275	450	
Water [kg/m^3]	187	193	Incl. extra water for higher liquidity
NCA 5/15 [kg/m^3]	960	1050	Natural coarse aggregate
NFA 0/2 [kg/m^3]	180	60	Natural fine aggregate
NFA 0/4 [kg/m^3]	725	574	Natural fine aggregate
Additive [kg/m^3]	1,73	4,10	
TOTAL MASS [kg]	102,49	102,83	Maximum concrete-mixer: 100kg

Table 4-3 - Composition of the definitive specimens

Fig 4-17 - Preparation of the concrete ingredients

4.3.2 Dimensions of the trial specimens

The initial dimensions of these beams were 850x100x100mm (LxWxD).

Once the decision to follow ACI 446 as a guideline was made, it seemed the easiest geometry to test (small, light) was 600x100x100mm. Luckily, the cross section could be kept and solely the length had to be adjusted. This was done using a large wet saw.

Fig 4-18 - Wet cutting of the trial specimens to length

4.3.2.1 Compensation of specimen self-weight

The specimens need weight-compensation to avoid unstable failure before the end of the test. There are two ways to do this in ACI 446; this specimen can be shortened, for spatial reasons for example, or doubled in length. The beam length *L*, or counterweights must be chosen so that a hogging bending moment mgS/32 < *M* < mgS/16 at mid-span can be ensured.

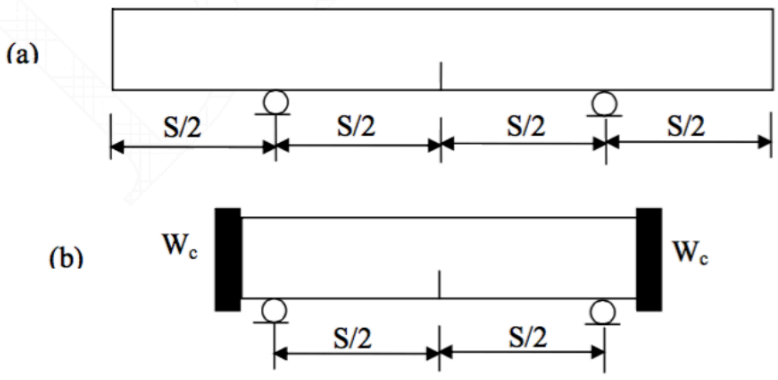

Weight compensation: (a) double-length specimen; (b) attached counter-weights.

Fig 4-19 - Weight compensation proposition in ACI 446

When following proposition (a), one will notice that it is impossible to satisfy the requirement for the hogging bending moment, as in that case it will always be 0:

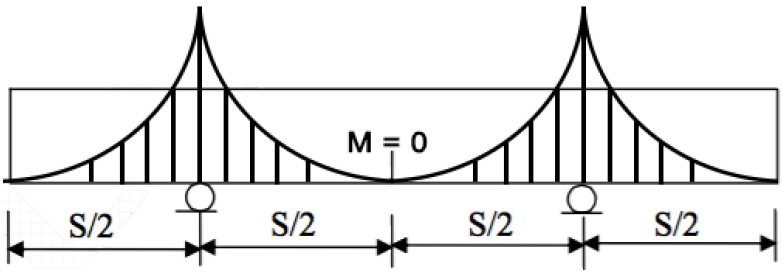

Fig 4-20 - Moment line of a double-length specimen

This is a point of discussion that should be consulted with the ACI 446 committee. The specimens that were tested for the purpose of this thesis were with double-length weight compensation, resulting in a moment-neutral point at the notch position.

4.3.3 Dimensions of the definitive specimens

No difficulties were encountered with the dimensions of the trial beams during testing, so the same recommended dimensions were kept for the definitive specimens: 600x100x100mm.

Fig 4-21 - Wooden moulds for the first concrete type (600x100x100mm)

NOTE: Although easy to make, wood seemed not to be the best option as material for the moulds. The concrete was allowed to expand a bit, resulting in some specimen's cross-sections not being perfectly square.

Fig 4-22 - Complete definitive C30 batch – Note: a standard cube replaced one cylinder

4.3.4 Notch depth, width and application method

No concrete instructions were available at the time of the trial as stated earlier, so for one trial specimen RILEM TC50-FMC was followed. This meant casting a notch equal to half the beam depth ± 5 mm [20]. For the second trial specimen, options were left open and no notch was casted. It was later cut by a large wet saw to 1/3 of the depth (= 33mm) with ACI 446 in mind. Both notches had a notch width of 5mm, which did not exceed the RILEM TC89-FMT recommendation of maximum 0.5 times the largest aggregate size (10 mm) [1]. This, however, does exceed ACI 446 recommendations (N < 0,02D = 2mm, see Fig 4-24 - Specimen geometry and dimensions).

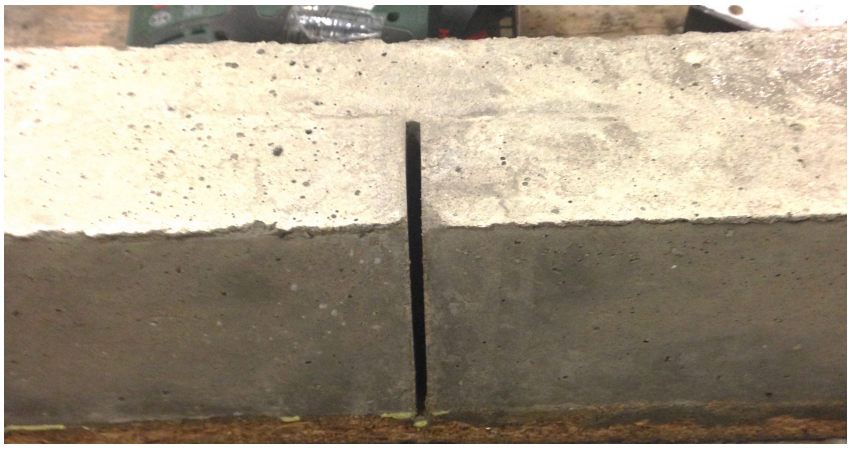

Fig 4-23 - Cast notch 0.5D and width 5mm instead of 2mm for first trial specimen

As remarked during the preparation of the 2 trial specimens, it was unclear what the ideal notch depth was, neither how this notch should be created. At the time of the trial specimens, 2 notch depths (1/3D and 0,5D with D being the beam depth) were made. These specimens were tested and the results were somehow acceptable (see Conclusions after trial tests). The definitive specimens could thus be prepared and the guideline to follow (ACI 446) had also been chosen. This lead to using a notch depth of D/3, or 33mm in our case:

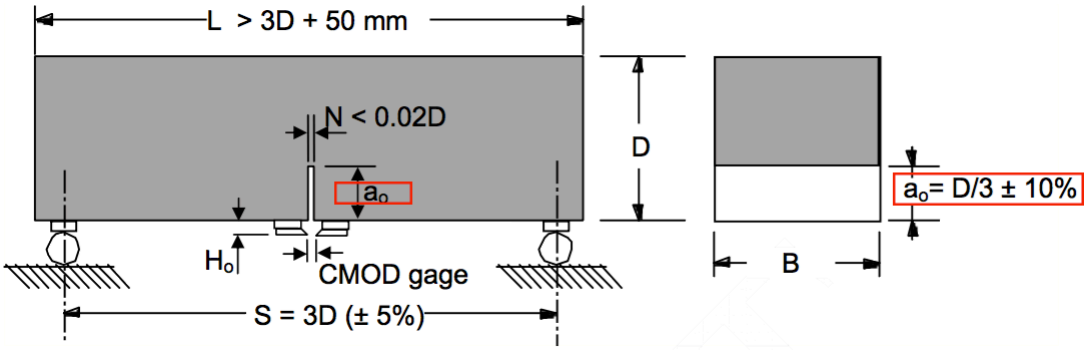

Fig 4-24 - Specimen geometry and dimensions [19]

The notches in the definitive specimens were cut dry, 26 days after casting, using an electrical handsaw with diamond disc with a 1.8mm thickness, resulting in a 2mm notch (which is equal to 0,02D, as defined in the ACI 446 guideline). In ACI 446 this method is described as *"Cut the notch using a circular saw so that the notch front is perpendicular to planes that were horizontal during casting. Use a diamond saw with water cooling and keep the pressure of the saw as low as possible to avoid damaging the concrete."* [19]. This is similar to the RILEM TC50-FMC recommendations where the notch is preferably sawn under wet conditions, but it may also be cast if a suitable saw is not available [20]. Since casting the notch had given some complications and difficulties when unmoulding the trial specimen, cutting the notches after the concrete hardened was preferable in our case. No wet saw with the correct thickness was available, dry cutting was necessary.

4.3.5 Curing

Regarding the curing of the concrete specimens, ACI 446 recommends [19]:

6.4. *Casting, Curing and Conservation:*

6.4.1 After demolding, cure and conserve the specimens in a lime saturated bath at 23 ± 5 ° C until testing time.

6.4.2. After removal of the specimen from the bath, and until the end of the test, drying of the surface of the specimen shall be prevented. A wet cloth and/or a spray bottle may be used to keep the specimen surfaces damp.

Fig 4-25 - Proposed curing method

This curing method could not be fulfilled for 2 reasons:

- There is no curing bath in UdG. Instead, the specimens were kept on large plastic sheets, covered by jute cloths of the same size, with another layer of plastic to cover it all. The jute rags were excessively watered every 1 or 2 days, so the concrete was wet at all times. This was the case until 3 days before testing.

- Because DIC was going to be used, it meant that on each specimen, one side surface had to be painted white just before testing. Therefore the specimens had to start drying 3 days before.
- Since the specimens were dry after painting, they were kept that way. For no specimens drying of the surface was prevented.

4.3.6 Compressive & tensile strength

This batch of concrete for the trial tests was expected to be C25. Two cylindrical compression tests were performed. This gave 2 peak loads; 331,8kN and 313,1kN; given an average diameter of 150mm, this results in respectively 18,78MPa and 17,72MPa. The average of 18,25MPa was used in calculations. No tensile strength tests could be performed for the trial specimens, so an approximate 10% of the compressive strength was used.

Regarding the definitive specimens, 4 tests were performed for the 3 specimens:

- 1 cylinder: Tensile test
- 1 cylinder: Compression until rupture
- 1 cube: Compressive test (until rupture)

Average compressive strengths of 25,25 MPa were found for the C30 specimens. Brazilian splitting tests were also performed to determine the average C30 tensile strength: 2,62 MPa. For the C50 specimens, an average compressive strength of 58,30 MPa was assessed and a tensile strength of 3,37 MPa.

4.3.7 Resume of used specimens and settings

Specimen	Notch Depth [mm]	Notch Width [mm]	Notch Method	Curing	Compr. Strength [Mpa]	Tens. Strength [Mpa]	use of DIC technique	Used machine	Load point displacement speed [mm/min]	Peak load [N]	Considered successful test
Trial_C18_1	33	5	large saw wet cut	wet cloths	18,25	1,83	-	MTS Insight 100kN in AMADE lab	0,06	3009	v
Trial_C18_2	50	5	cast				-		0,10	1668	v
C30_1	33	2	hand saw dry cut		25,5	2,62	v		0,11	4670	-
C30_2	33	2	hand saw dry cut				v		0,06	4571	-
C30_3	33	2	hand saw dry cut				v		0,01	4620	-
C30_4	40 [1]	2	hand saw dry cut				v		0,01	3717	-
C50_1	50 [2]	5	large saw wet cut		58,6	3,37	-	Str. Lab [3]	0,06	4227	-
C50_2	33	2	hand saw dry cut				-		0,05	5200	improvement [5]
C50_3	33	2	hand saw dry cut				-	MTS 858 [4]	CMOD ctrl	-	did not work [5]
C50_4	33	2	hand saw dry cut				-	untested [5]	-	-	untested [5]

[1] Hand sawn after 33mm, see later
[2] Attempt to decrease bulk energy, see later
[3] 600 kN capacity with 100 kN load cell
[4] *MTS 858 Table Top System 25 kN capacity*
[5] See chapter 5.2

Table 4-4 - Resume of used specimens and settings

5 Experimental results

Before testing definitive specimens two trial tests were performed, because very little was known about the conduct of three-point bending tests to assess fracture properties. Not only machine settings, but also results and points of improvement to the test setup were interesting. These trial tests were performed without the use of the digital image correlation (DIC) technique, because the reference frame with HLS sensors needed testing to compare with the machine's LPD registration.

5.1 Test results

The two trial tests where submitted to the three-point bending test without the use of the DIC technique, as this was not a priority. For the definitive specimens, all C30 beams were monitored with the DIC technique, whereas this was not the case for any C50 specimen because enough results with DIC were obtained to form conclusions.

Results are divided per specimen, with only the most important data in this chapter.

5.1.1 Trial_C18_1

NOTE: For this test the loading block was not the correct one yet (see Fig 4-11 - Difference between 2 loading blocks), although this did not seem to affect the test significantly.

The whole goal of these trial tests, as mentioned several times throughout this thesis, was becoming familiar with the conduct of the test.

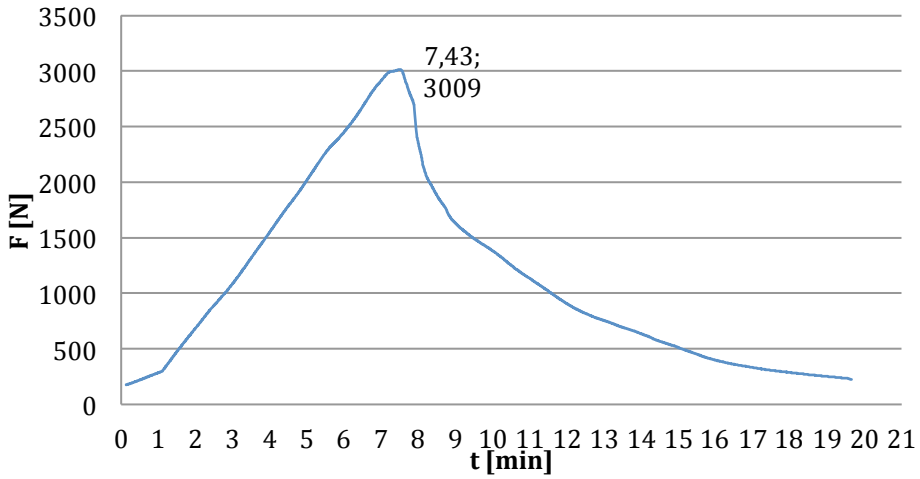

Graph 5-1 - Load vs. time Trial_C18_1

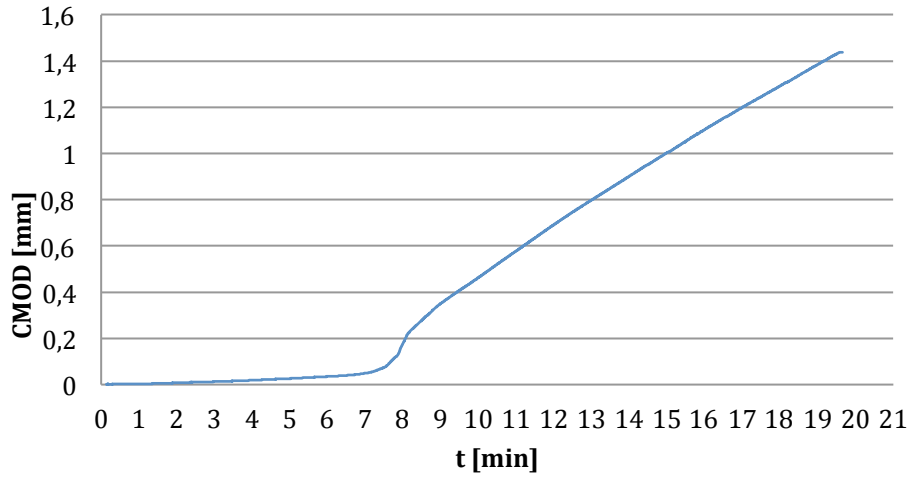

Graph 5-2 - CMOD vs. time Trial_C18_I

As can be seen, the peak load was only reached after seven minutes. This means the test should be considered invalid according to ACI 446 (since the peak load should be reached between 3 and 5 minutes to keep the length of the test acceptable) [19]. In our case this did not affect the conduct of the test.

Note that the relation between load and CMOD is also very clear when looking at both curves. Whenever the peak load is reached, the crack opening increases more rapidly.

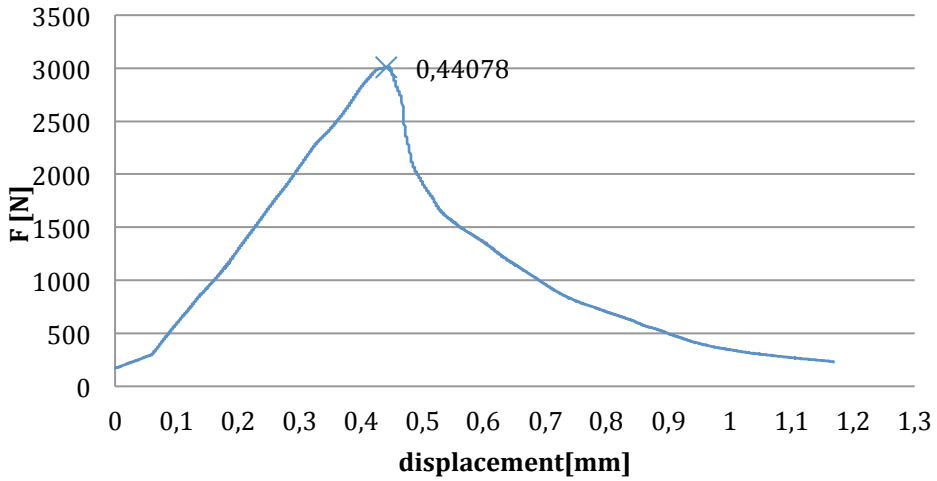

Graph 5-3 - Load vs. displacement Trial_C18_I

To determine the corrected load rate for the second trial, it was calculated using above curve, by taking the mean time needed to reach the displacement (≈ 0,44 mm) at the peak load. The peak load should be reached anywhere between 3 and 5 minutes, so the calculated speed was based on a time of 4 minutes (= 240 s).

$$LPD\ rate = \frac{load\ point\ displacement}{time} = \frac{0{,}44}{240} = 0{,}0018\frac{mm}{s} \approx 0{,}10\frac{mm}{min}$$

Of course, the main interest of the test is obtaining the load vs. CMOD curve:

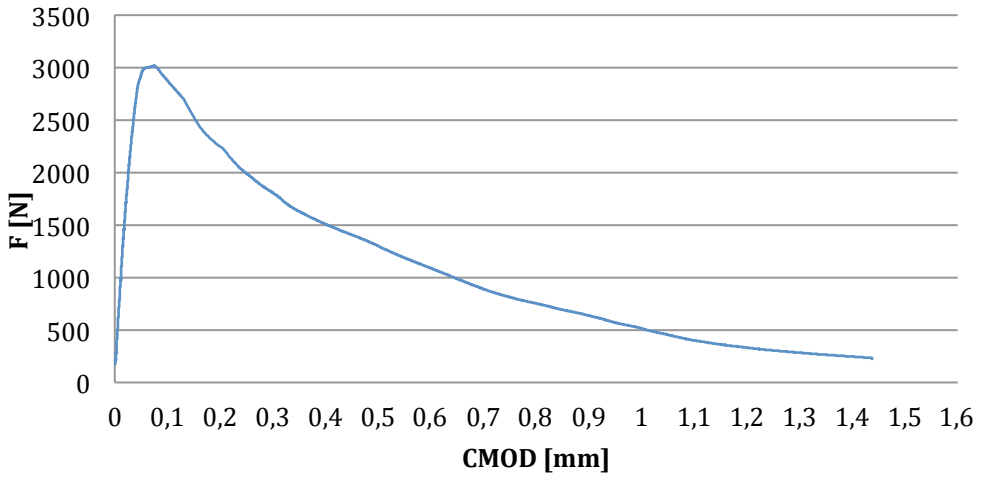

Graph 5-4 - Load vs. CMOD Trial_C18_1

This curve looks like the found curves in studied papers. The question of why testing with CMOD control instead of (constant) load point displacement speed was needed rose. This will become clear after testing the definitive specimens.

5.1.2 Trial_C18_2

NOTE: After testing the first trial with a 33 mm notch, and cutting the 8 definitive specimens with a 33 mm notch, it was completely overseen that this second trial specimen had a cast notch of 50 mm. Because of this, the peak load was of course much lower than expected and reached too soon, as the load point displacement rate was calculated for a 33 mm notch. The resulting curves and values are nevertheless still similar, as below curves will show.

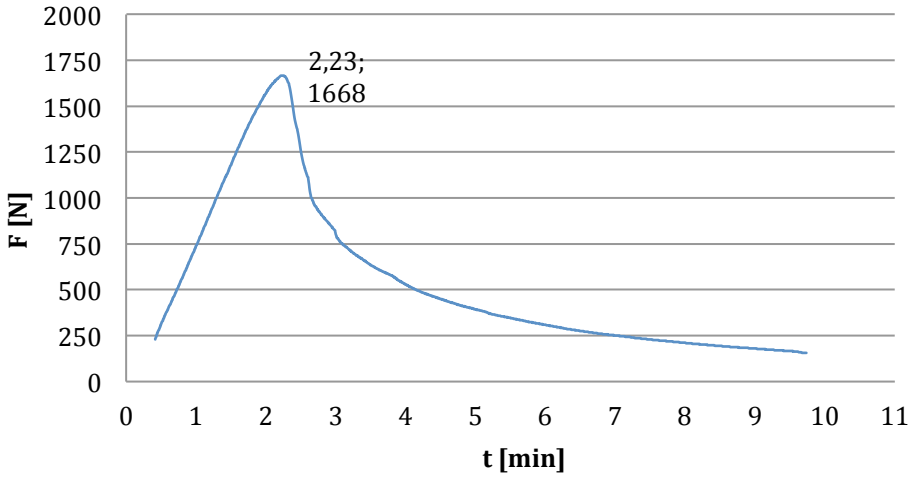

Graph 5-5 - Load vs. time Trial_C18_2

Peak load was approximately halved compared to the first trial because of the larger notch, and reached after some more than two minutes. Again, this test would be considered invalid when following ACI 446. The pre-load of 240 N (8% of 3000 N) was still within the maximum of 15% of the actual peak load (= 0,15x1668 = 250 N) though.

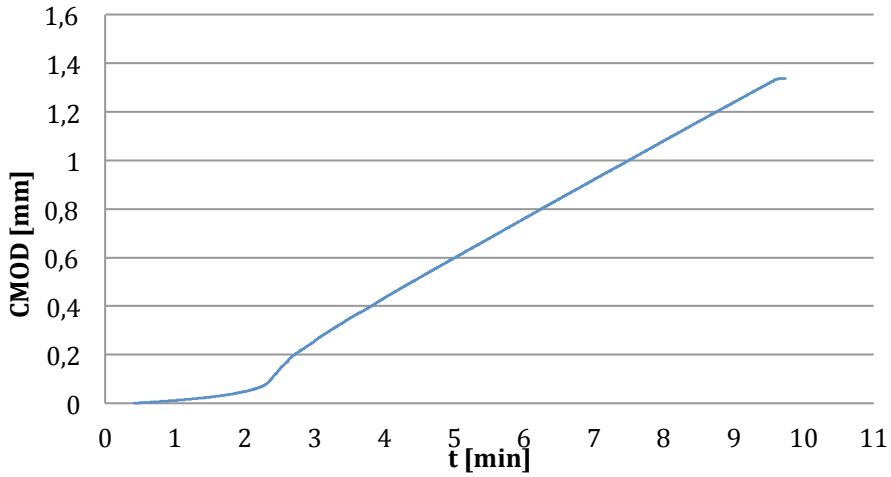

Graph 5-6 - CMOD vs. time Trial_C18_2

Again, the same relation between CMOD and (peak) load can be seen when comparing both curves.

The obtained load vs. CMOD curve was also similar to the first test:

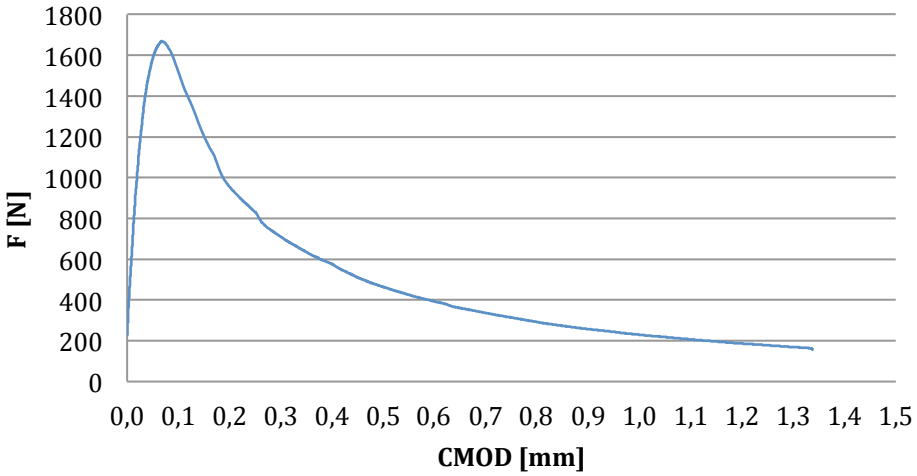

Graph 5-7 - Load vs. CMOD Trial_C18_2

5.1.3 Comparison of HLS and LPD measurements

Another interesting curve that was obtained for both trial specimens is the LPD and HLS comparison. For trial 1 these results were rather confusing, considering the values of one HLS (HLS 25/09) go under 0 (meaning the beam would bend upwards on that side) and are very oscillating. The large and increasing difference between both HLS sensors is probably due to the beam not being perfectly square but trapezium-shaped because of the concrete moulds expanding during curing. This would result in the beam leaning to one side more than the other. Using the incorrect loading block (too short, not perfectly centred?) probably also has a role in this. Curves for the second trial test were easier to interpret.

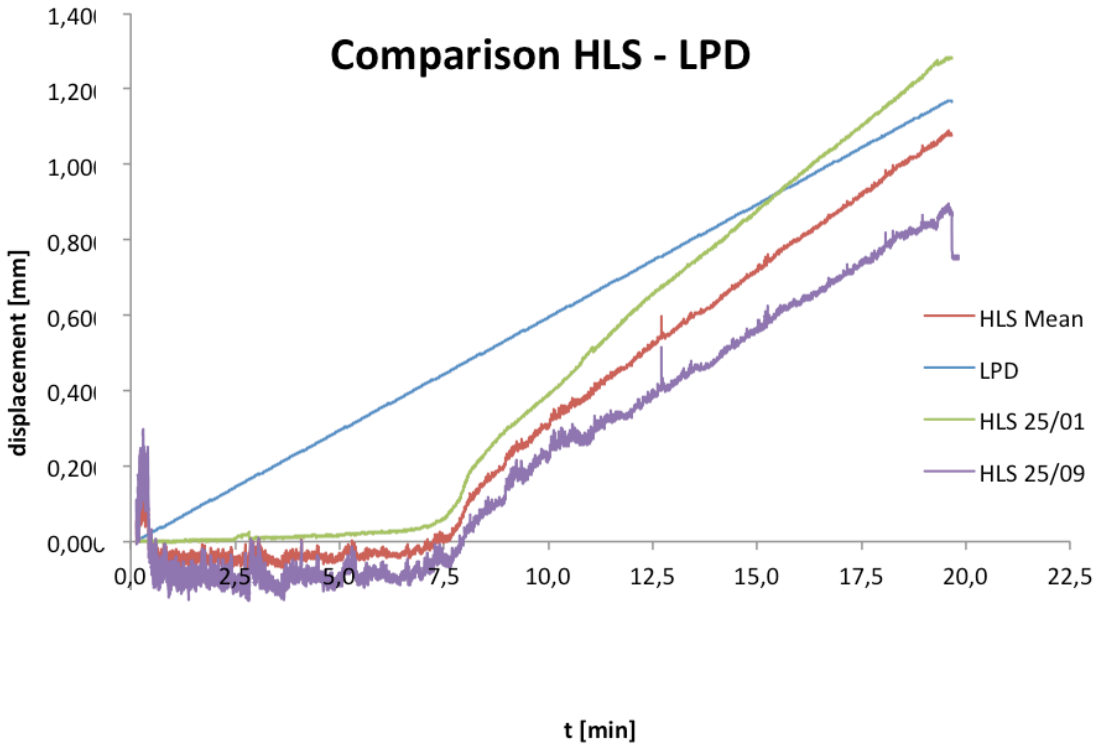

Graph 5-8 - Comparison of the measured displacements by the HLS devices and LPD for Trial_C18_1

Comparison of HLS and LPD for the second trial is represented in below graph:

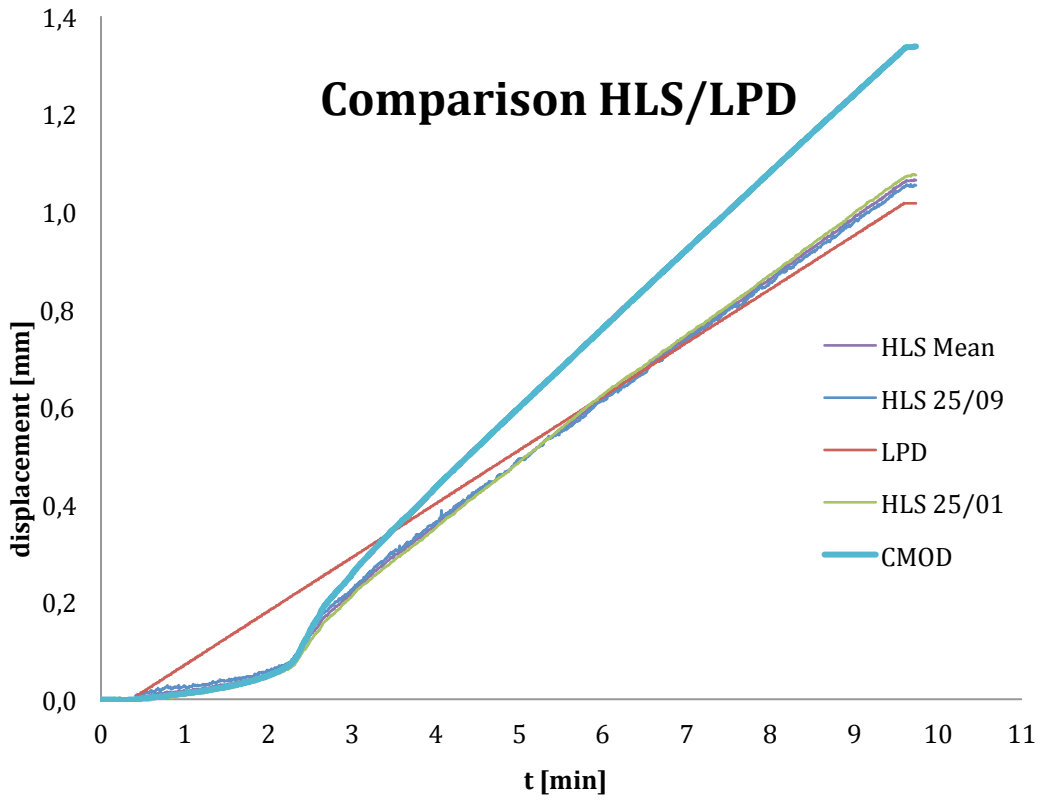

Graph 5-9 - Comparison of the measured displacements by the HLS devices and LPD for Trial_C18_2

Here, the results were clearly much better and consistent. Both sides of the beam had the same displacement when looking at both HLS devices (no leaning to one side like for the first specimen). The same trend as in the first trial can be observed: staying close to no displacement before the peak load, and then increasing more rapidly after it.

The question was if the testing machine's LPD could be trusted, meaning simplifying the test setup by not using the reference frame with HLS's, or if the load point displacement should better be measured using the HLS's (as recommended in ACI 446). LPD was accurate according to AMADE quality system. The difference between HLS and LPD results is partially due to the tilting of the beam as said above. For the second trial, the CMOD vs. time has been added to the graph. This shows an interesting fact: there is a relation between the displacement registered by the HLS's and the crack opening. This means the difference between HLS and LPD may be justified by the place of measuring.

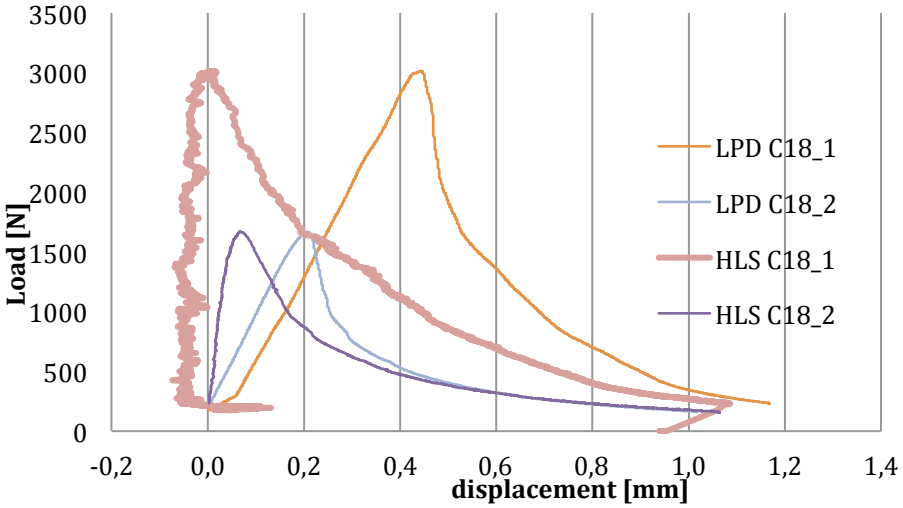

Graph 5-10 - Load vs. LPD and HLS displacement for both trial specimens

As can be seen, the HLS (measured with the bottom of the beam as displacing point) stays close to 0 until the peak load is reached. Once the beams cracks, the bottom has a large (increasing) displacement because the stiffness of the beam has decreased. A solution to this difference between both measurements could be turning the reference frame upside-down, and using the HLS's to measure the displacement at the top of the beam. This has not been done during this thesis but should be tried.

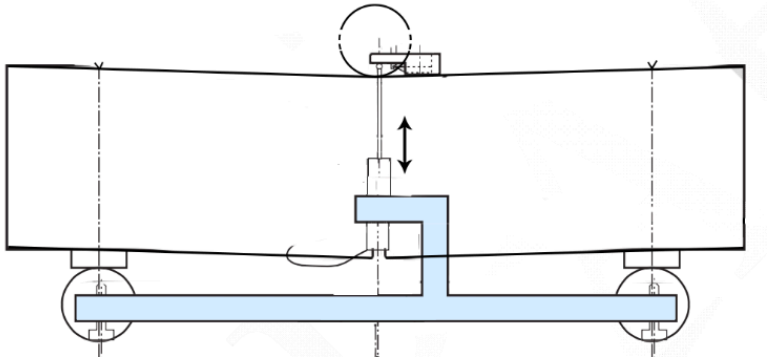

Fig 5-1 - Presentation of proposed solution for load point displacement measuring

5.1.4 Conclusions after trial tests

Both trial tests were stable so the found curves seemed acceptable.

5.1.5 C30 specimens

For the first following tests, the DIC technique was going to be applied, so the reference frame (thus HLS's) was not be used. Graph 5-11 shows LPD vs. time for all specimens. The drops in the C30_4 curve are explained later. The large difference in displacement rate between 2 couples of curves (C30_1&2 and C30_3&4) lead to using different time scales in Graph 5-11 and Graph 5-12.

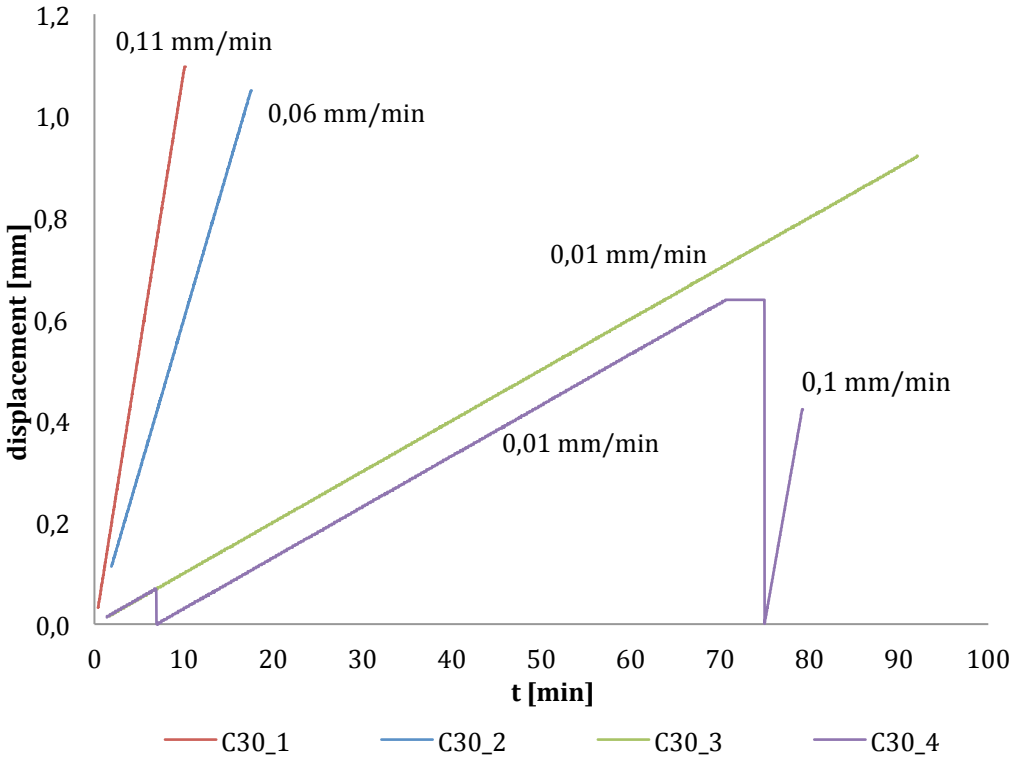

Graph 5-11 - Comparison of load rates for C30 specimens

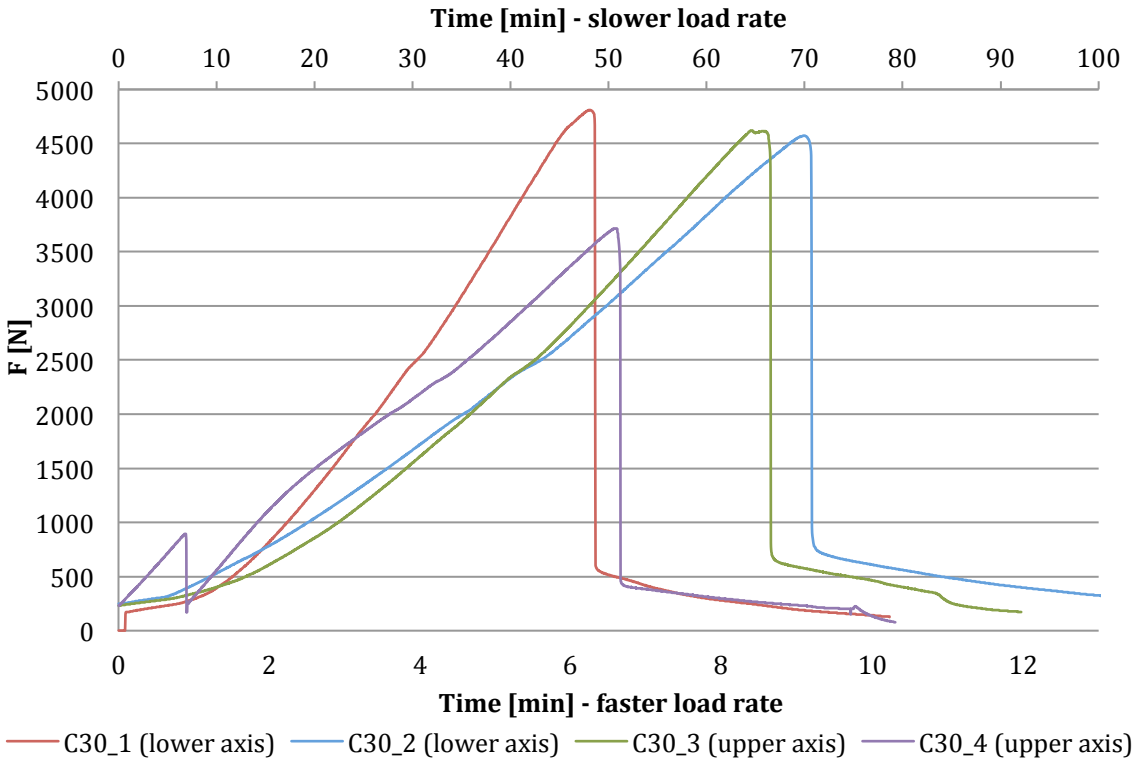

Graph 5-12 - Load vs. time for C30 specimens

All specimens suffered sudden cracking, resulting in unusable data. The load point displacement rates were only equal for C30_3 and C30_4, for this reason two time-axis' were used. In an attempt to make the specimens crack in a graduate way, the load point displacement speed was lowered.

NOTE 1: Because all previous tested specimens suffered from sudden cracking, an adjustment for C30_4 was made in an attempt to make it crack gradually. The notch was cut 10 mm deeper and narrower at the tip using a manual saw. The impact on the peak load is clearly visible in the graph.

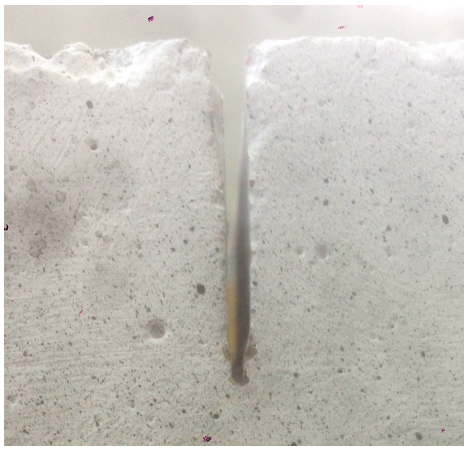

Fig 5-2 - Deeper and narrower notch tip C30_4

Alas, this had no effect on the behaviour of the crack during the test; see the sudden load drop on the curve.

NOTE 2: The test results for C30_4 have another inconvenience: because the test had to be stopped 2 times to adjust the load point displacement rate, the curves have several interruptions. These interruptions are also visible on the C30_4 curve. They are also visible in the CMOD vs. time curve:

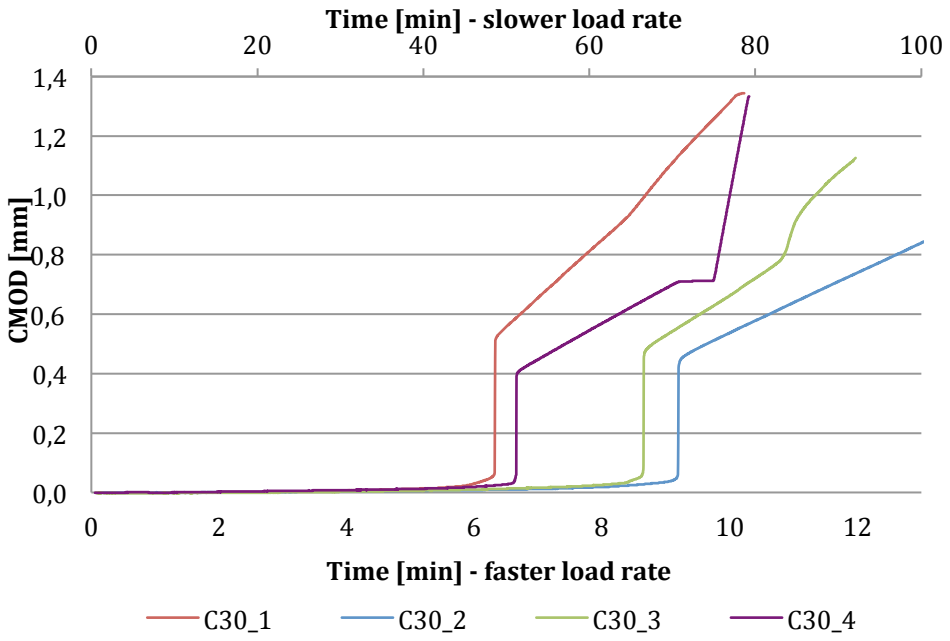

Graph 5-13 - CMOD vs. time C30 specimens

The change of CMOD rate for C30_3 is due to an internal concrete imperfection, like a large aggregate in the middle of the crack.

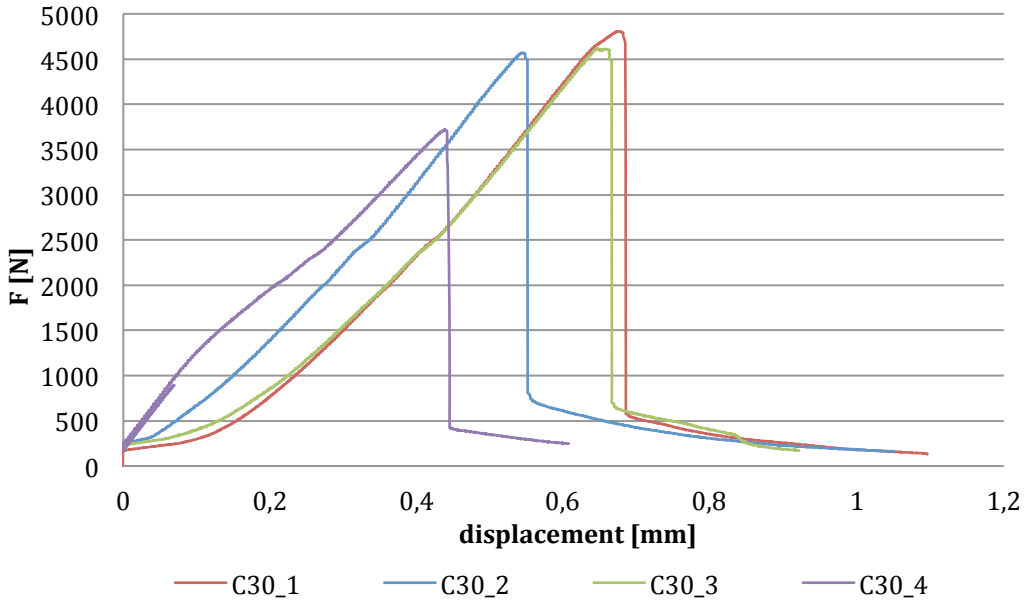

Graph 5-14 - Load vs. vertical displacement C30 specimens

The C30_2 specimen has been pre-loaded too much (to 900 N) before starting the test. The C30_2 curve does not coincide with C30_1 and C30_3 because at the very beginning of the curve the slope (= initial stiffness.) was greater, this could be a specimen imperfection. Later on, the slope is equally steep, meaning a similar stiffness. As for the shape of the C30_4 specimen: it has been pre-loaded several times because of stopping the test to change the speed, and then starting over. This could explain the shape of the curve up to the peak load. The lower peak-load is due to the larger notch as mentioned before.

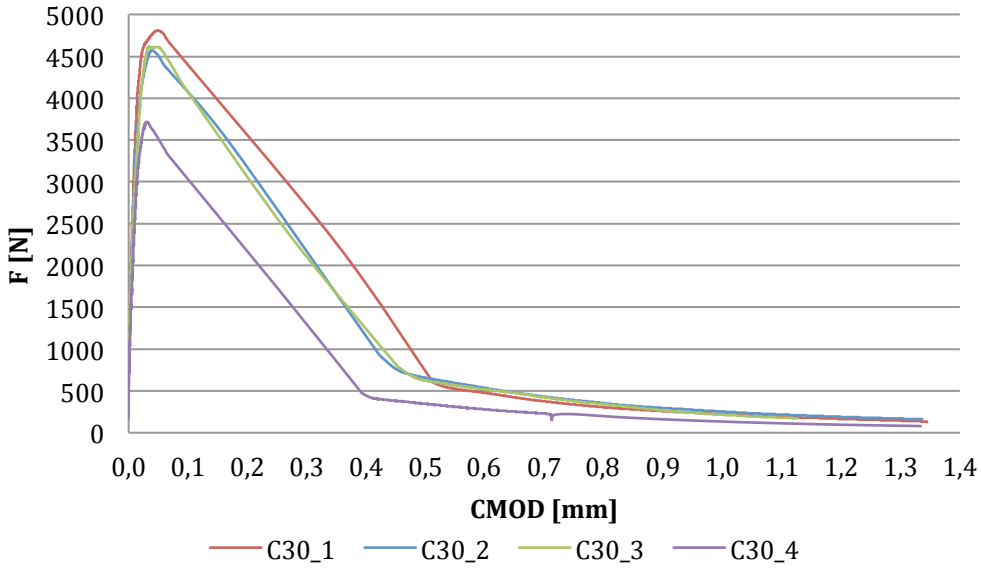

Graph 5-15 - Load vs. CMOD C30 specimens

All the curves are similar in shape, but unusable for further calculations for the fracture energy parameter due to the sudden crack, since it evaluates the area under the force-CMOD softening curve.

5.1.6 Analysis of three-point bending test results

Several reasons for the failure of all C30 tests were considered:

- Could the imperfection of the cross section (no 4 right angles) have a significant impact? Probably not on the sudden cracking, but this has to be taken into account when analysing results.
- The used cement type was CEM I 52,5R, whereas in other tests CEM I 32,5R is more commonly used. Also for the successfully tested trial specimens CEM I 32,5R was used. Did the stronger cement make the specimens too brittle? It was later learned that this should have no impact on the test [17].
- The specimens were not kept wet at all times; this must have had effect on the shrinkage strain. Could this have made the concrete more brittle?
- Were the notch dimensions and execution *correct*? As shown with C30_4 and later with C50_1 this seemed to be of little importance.
- The load rate and data registration frequency had no influence on the conduct and result of the tests. The stiffness of the machine is of importance and the compliance of the machine can cause unstable effects (5.2).
- The closed-loop CMOD control would improve the stability of the test.

5.1.7 DIC results

Once all the pictures taken during a test are calculated (positions of all points and strains) in *VIC-3D* or *VIC-2D,* they can be manually analysed. In the calculated and rendered square section, dots can be placed wherever and all information about that dot can be extracted, dot-by-dot (another small flaw, since extracting information can require quite some time; it would be handier to select multiple dots and extract all info at once). For the CMOD for example, couples of dots were placed at different heights of the beam. An abstraction of both dots gives the evolution of the distance (= notch or crack opening) between two dots over time.

5.1.7.1 C30_1 (3D)

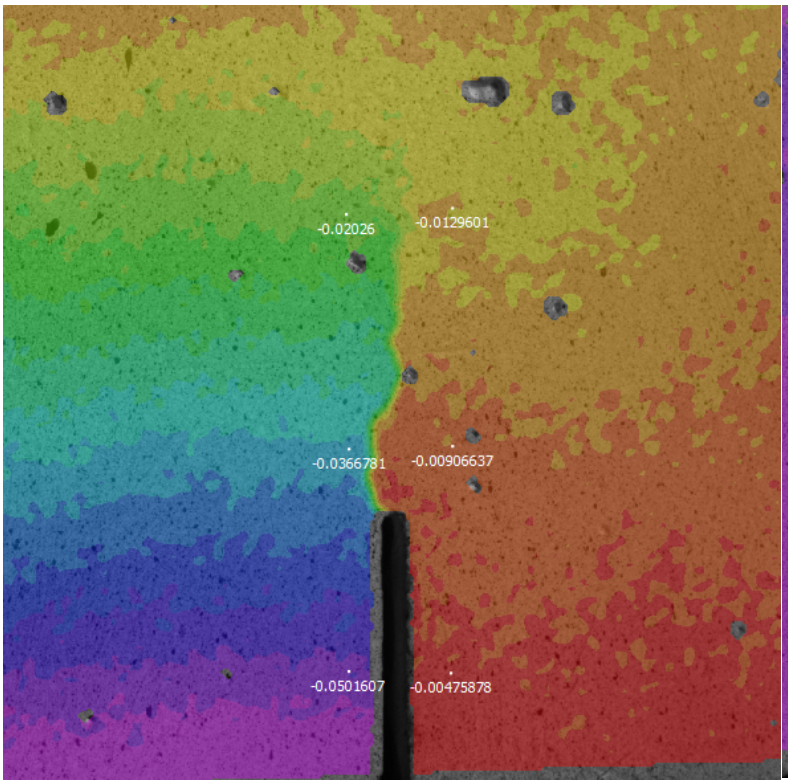

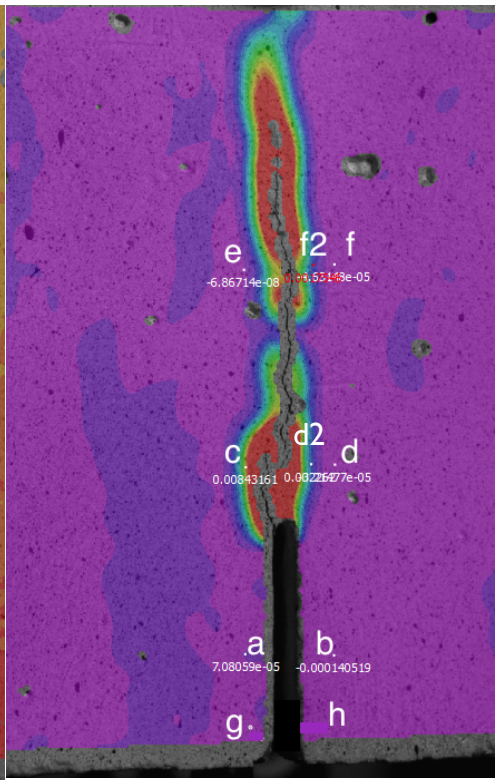

Fig 5-3 (left) - Displacement in X-direction just before cracking, C30_1

Fig 5-4 (right) - Strains in X-direction after cracking, C30_1

These images are interesting to see, but of course the real interest is in the calculated curves and comparison with results from the 3PBT (synchronisation explained in 4.2.1.1).

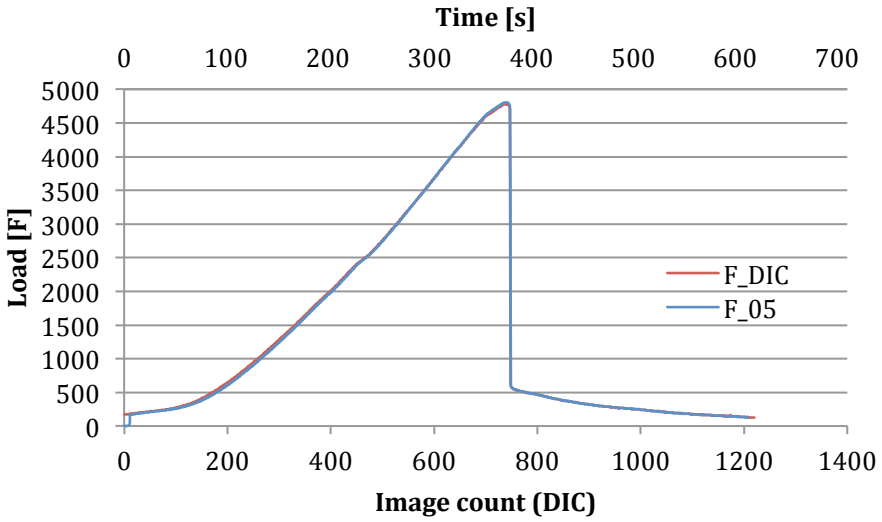

Graph 5-16 - Load vs. time and image count C30_1

This graph shows both time axis' (image number and real time) are perfectly synchronized. One can also deduce the photographing frequency, namely 2 images per second. This is the reason the force from 3PBT is called F_05, referring to one value every 0,5s. The following graphs are now comparable.

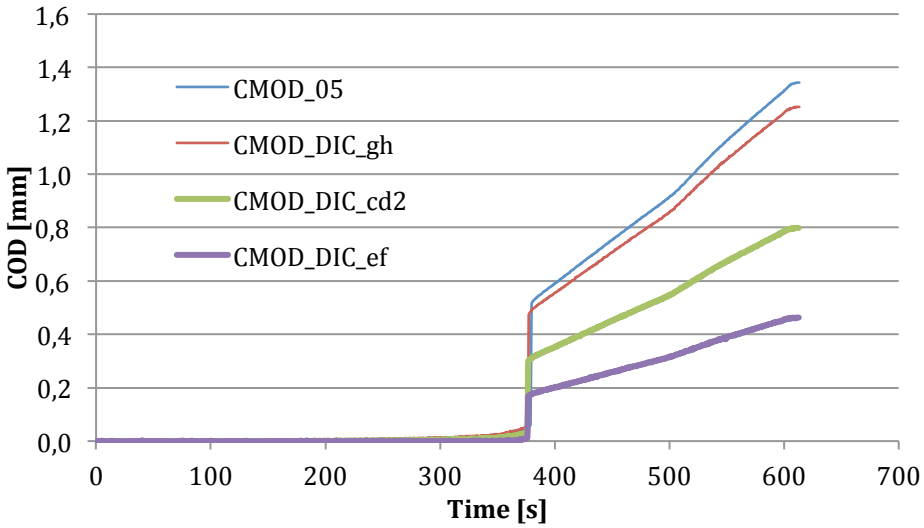

Graph 5-17 - Crack opening vs. time C30_I

One will notice there is a growing difference (0,1mm at the end of the test) between the CMOD registered by the extensometer and the COD between *g* and *h* calculated via DIC. This is due to the extensometer being placed lower than the actual notch opening because of the knives' thickness. As an extra, the COD between points *c* & *d2*, and *e* & *f* are also included to show the trend of the crack opening to the crack tip. Logically, for *e* & *f* this value is much smaller. Closer to the top of the beam the crack opening is almost 0.

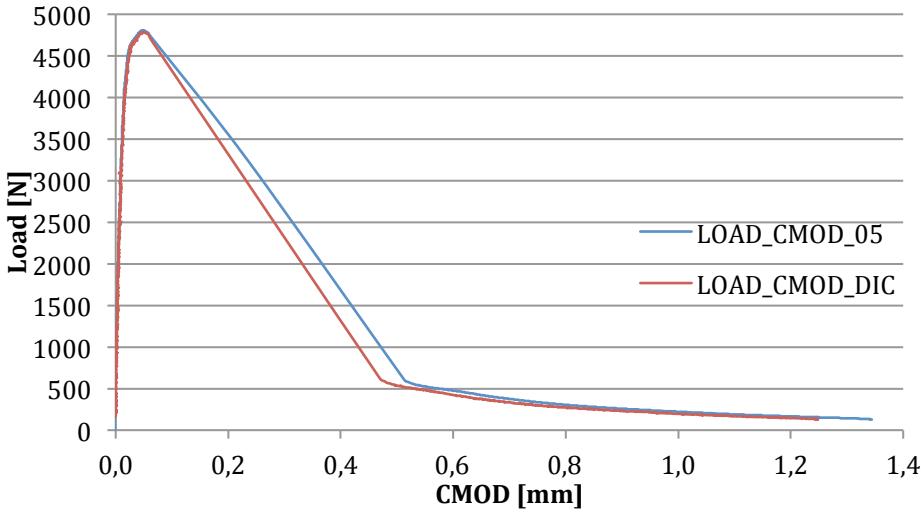

Graph 5-18 - Load vs. CMOD (with DIC: points *g* and *h*) C30_I

Using DIC has not solved the problem of the "missing" data due to the sudden crack (and thus drop of load). This is why between the peak load and 500 N the curve is linear, but should not be. Note that the small difference in crack opening due the height difference of measurement points is also clear in above graph.

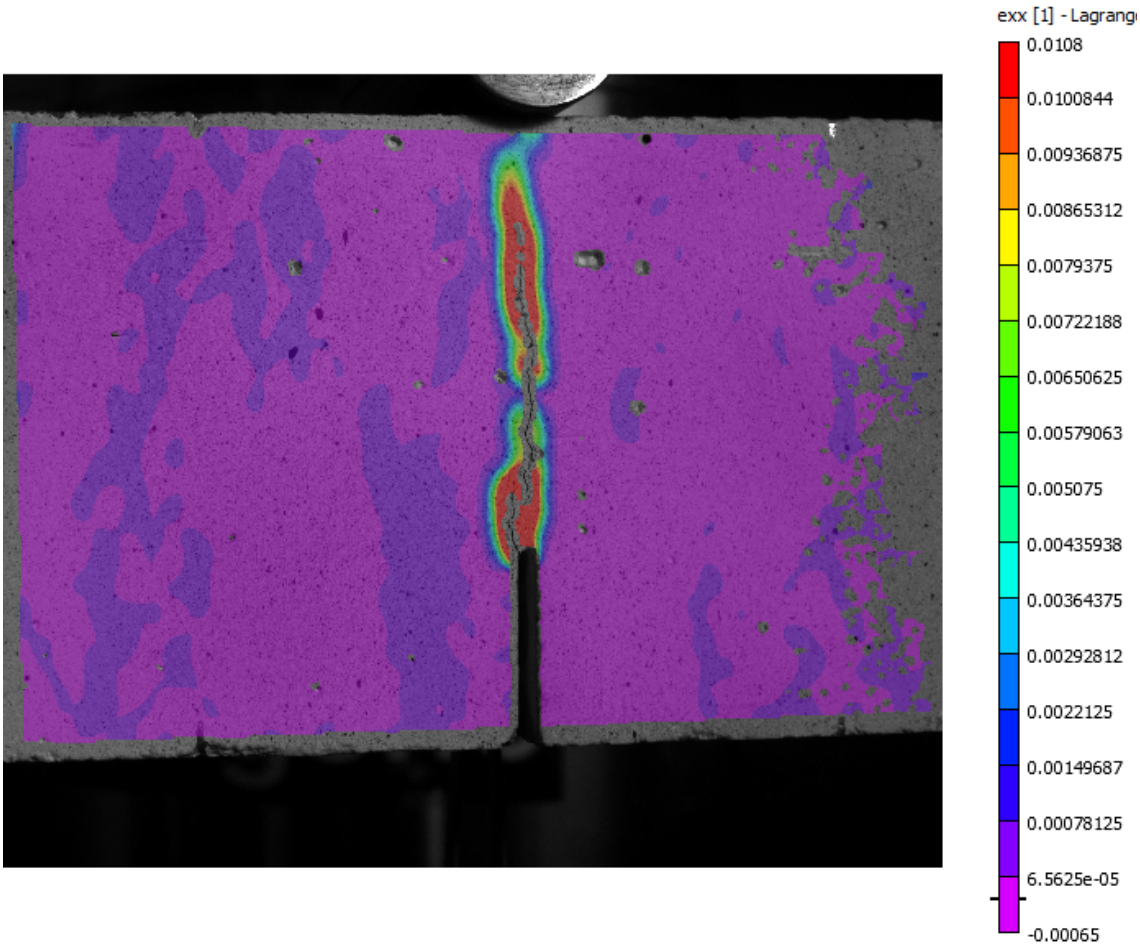

Fig 5-5 - Rendered strains for C30_I showing unrealistic results

Normal concrete rarely has strains higher than 0,008 after hardening (≈28 days) [25], whereas the DIC render shows strains largely exceeding this value. This makes it necessary to ignore these results. Although DIC has been successfully used in reinforced concrete members to study cracking and deflections [26], very limited literature is available on quantitative strain analysis [27].

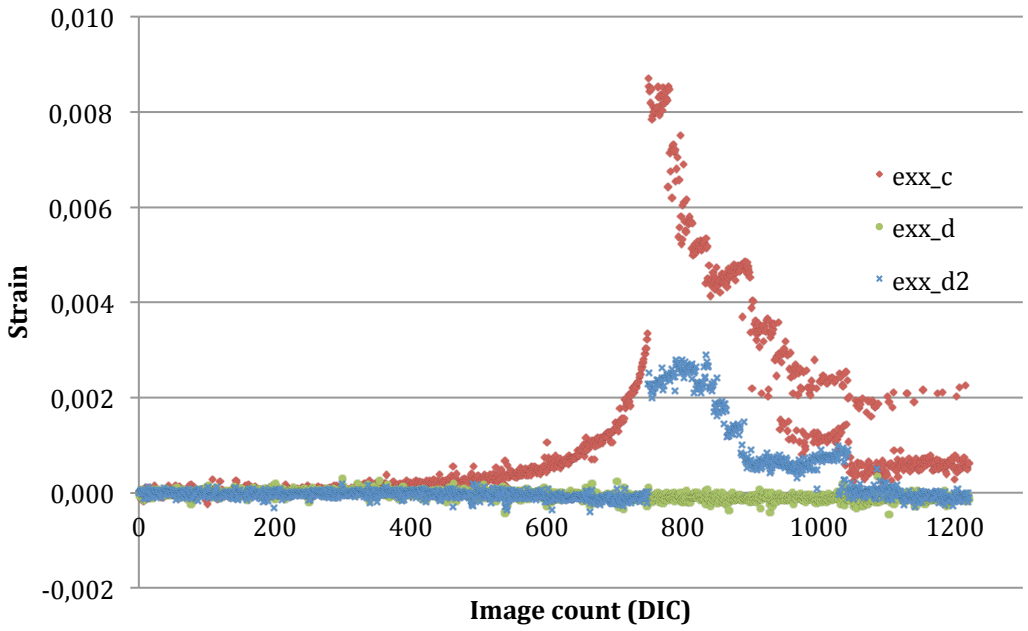

Graph 5-19 – Evolution of strains of different points C30_I

The evolution of strain in point *c* is, as in Fig 5-5 - Rendered strains for C30_I showing unrealistic results, unrealistically high. It is more acceptable in point *d2*, which is not in a red zone. Point *d*, situated relatively far from the crack, has strains fluctuating around 0, which can be assumed as correct. The conclusion is that calculated strains close to the crack are inaccurate, but unfortunately the most essential for a deeper understanding of the concrete behaviour.

To illustrate the extensive possibilities of the DIC technique, the followed path of points *e* & *g* are plotted:

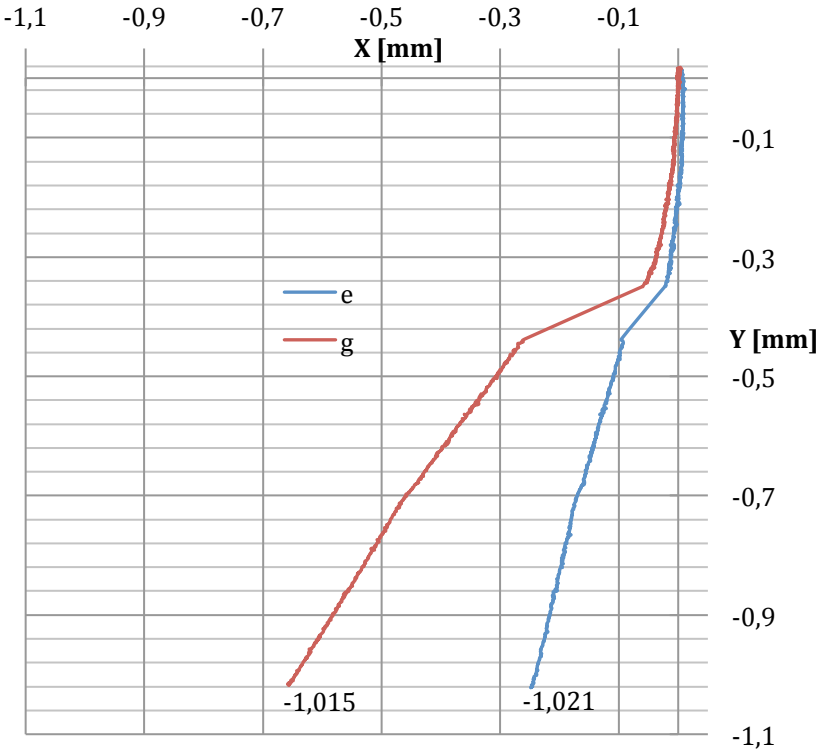

Graph 5-20 - Displacement of points, C30_1

As expected, point *g* has a larger horizontal displacement than e due to being at the lower end of the crack opening. What is remarkable is that a (although very small) difference in vertical displacement is visible. Logically it is point *g* that has a smaller vertical displacement. This shows that for displacement tracking, (3D) DIC can be very accurate.

5.1.7.2 C30_2 (3D)

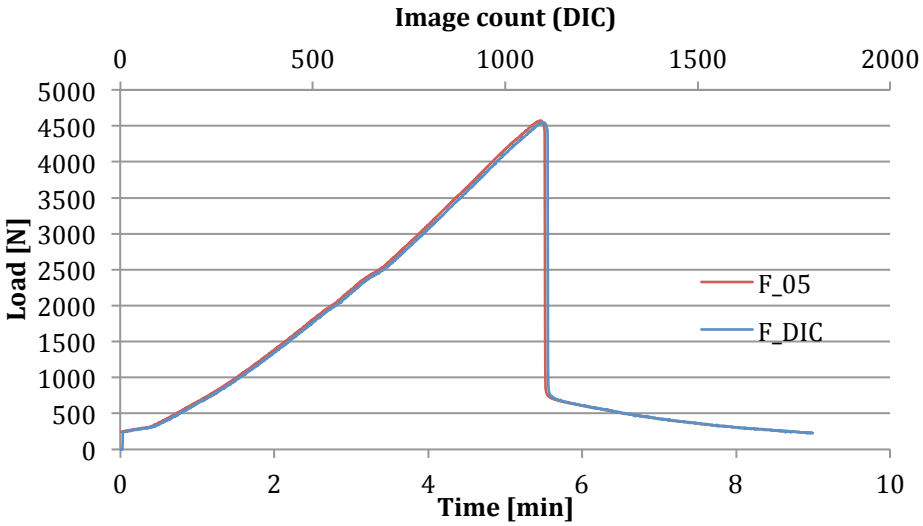

Graph 5-21 - Synchronisation of DIC and 3PBT registrations, C30_2

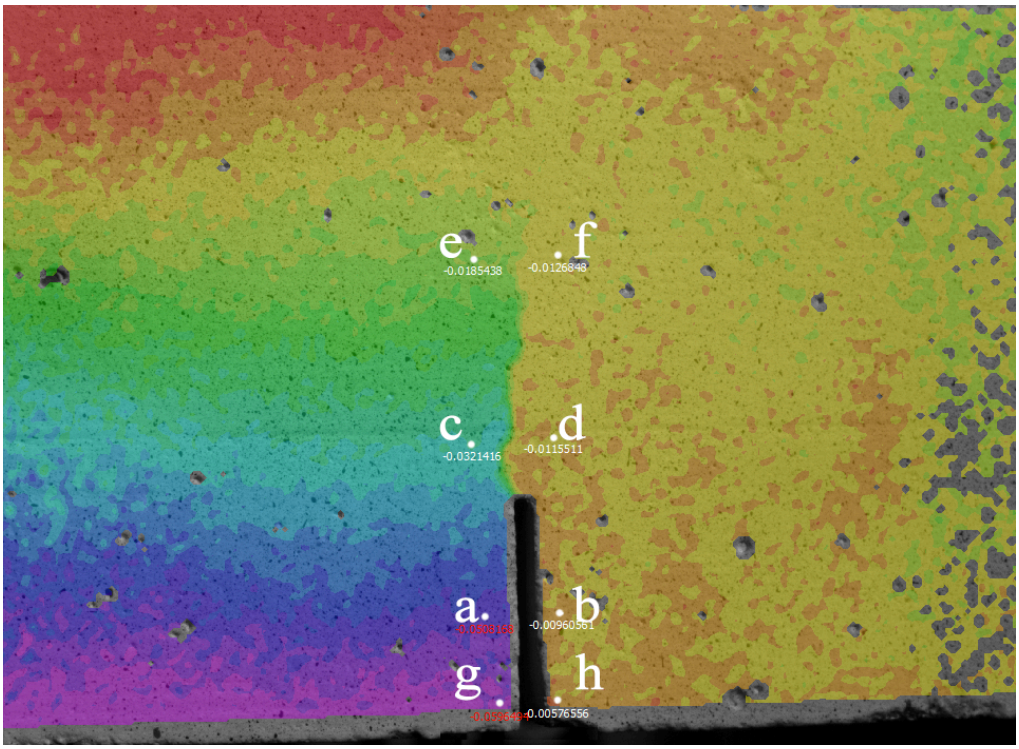

Fig 5-6 - Horizontal displacement just before the sudden crack, C30_2

Just like for the C30_1 specimen, the strains were beyond normal values. The displacements are correct though.

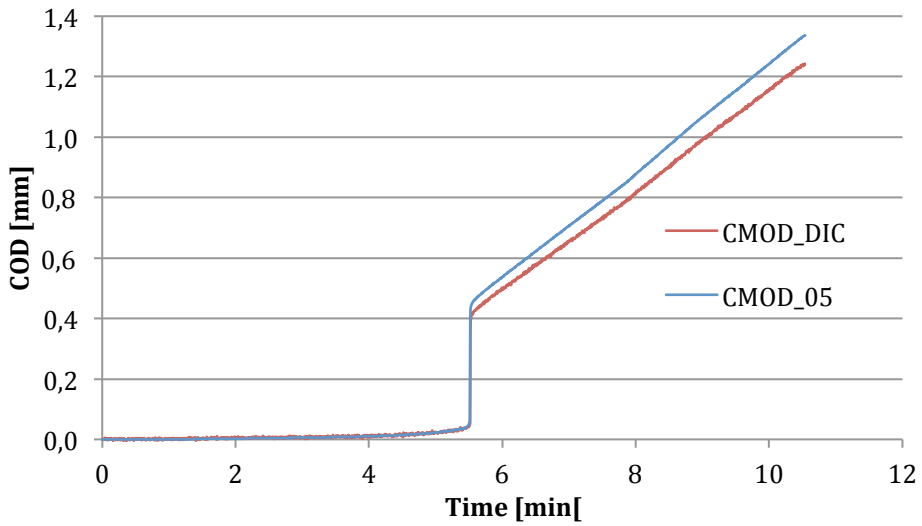

Graph 5-22 - CMOD vs. time C30_2

The same trend as for C30_1 can be seen. The difference in COD at the end of the test is 0,092 mm, almost identical as for the C30_1 specimen.

The load vs. CMOD curve was again unusable due to the sudden cracking.

5.1.7.3 C30_3 (2D)

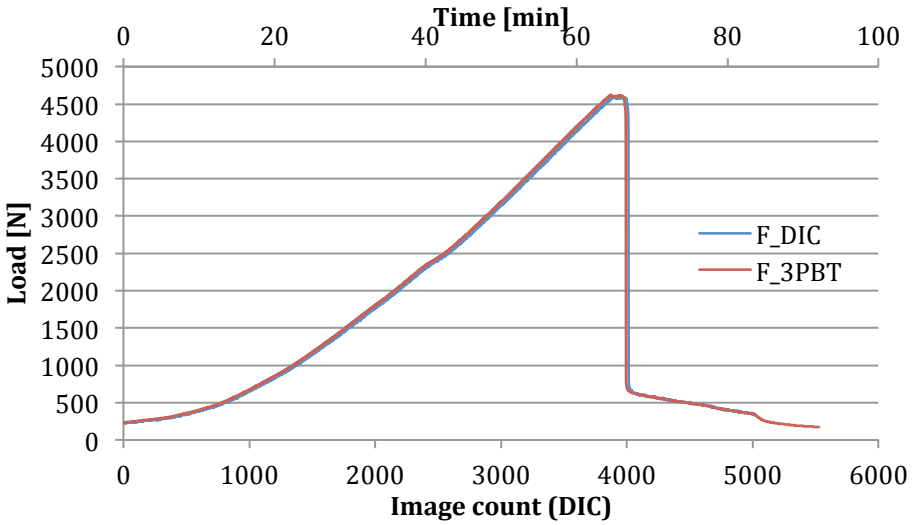

Graph 5-23 - DIC and 3PBT synchronised C30_3

Further data could not be analysed because the displacement registration of several points was incorrect. Values up to 8 mm for the horizontal displacement were calculated in VIC-2D for point *g* and *h (same coordinates as previous specimens)* for example, resulting in a crack mouth opening of more than 1 cm! This could be due to either a bad 2D calibration or very important out-of-plane deformations (unlikely). Not enough other 2D tests are available to be sure.

5.1.7.4 C30_4 (2D)

Graphs for the C30_4 specimen were not obtained due to multiple changes of the settings of both DIC and 3PBT setups (see 4.2.1.1). This resulted in fragmented curves that needed too time-consuming manual synchronisation. The conduct of the test was the same as previous specimens (sudden crack), so no important data is missing. The same problem occurred regarding displacement calculations, leading to unreal crack openings.

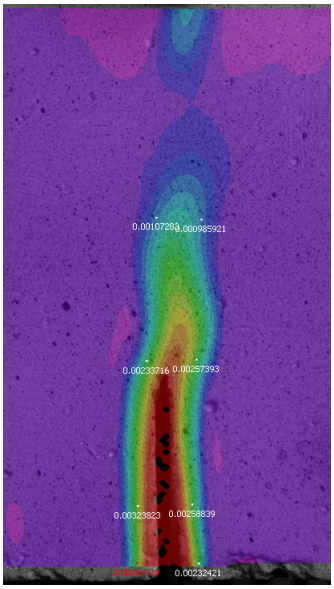

Fig 5-7 - Horizontal strain render C30_4

Interesting: At the top of the beam strains are appearing due to the pressure of the loading point before cracking. The renders of strains using DIC are correct in the sense that they represent what is happening at the surface of the beam, but the numerical values seem completely erroneous.

5.2 Revision of the test setup and remaining specimens

Because all C30 specimen tests failed, even with minor changes like increasing the notch depth, a solution had to be found before testing the even more brittle C50 specimens. Using a closed-loop CMOD control machine was needed. This was not easy in our case since such machine and accompanying programming were not immediately available. Also, the previously used machine's stiffness was not enough, this is very important. A sufficiently stiff machine had to be used [2], [3], about 10 kN/mm [1], with the goal of encountering less load-point displacement stability problems.

5.2.1 C50_1

Before a new machine setup could be tested, a C50 specimen was tested with previously used machine anyway. Only, this time, the notch was made much larger and deeper. It was re-cut using the large wet saw, to a depth of 50 mm and a notch width of 5 mm. This was done with the idea of keeping the bulk energy dissipation small [11]. This did not prevent a sudden crack though.

As an estimated peak load, only 4000 N was used (due to the larger notch). The pre-load was 290 N and the displacement speed was 0,06 mm/min.

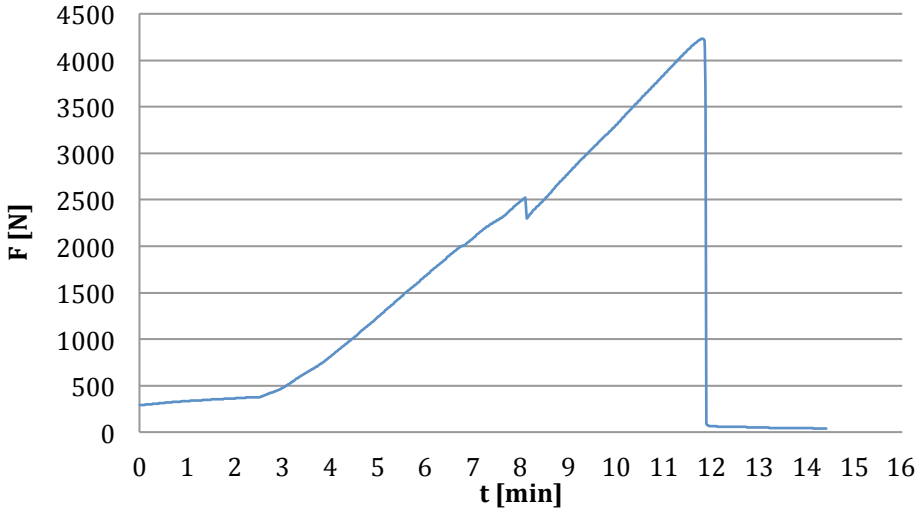

Graph 5-24 - Load vs. time C50_1

The sudden crack clearly appears at the 12th minute. The small drop at minute 8 is due to an imperfection of the beam at one of the supports. This data is without a doubt unusable for further calculations of the fracture mechanics parameters.

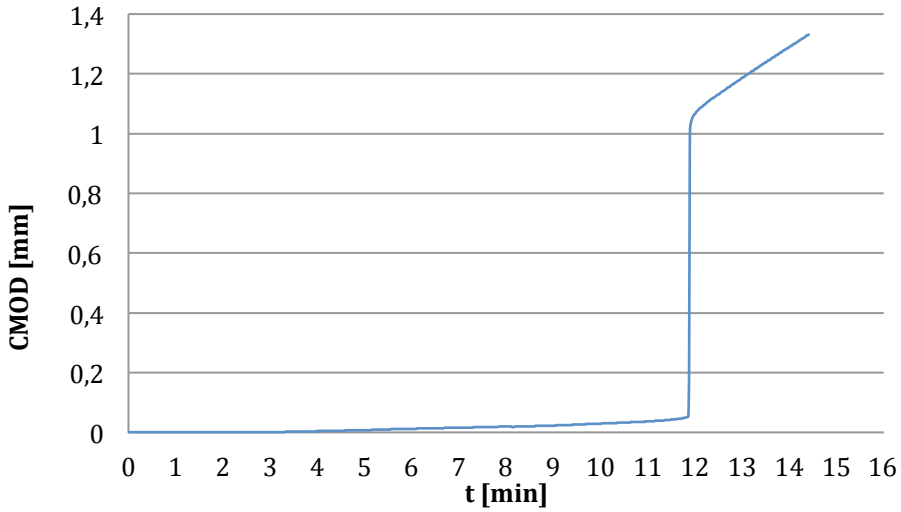

Graph 5-25 - CMOD vs. time C50_1

This sudden crack is somehow remarkable; the crack width increased almost one millimetre at once.

The load vs. CMOD curve is shown to point out its uselessness for further calculations:

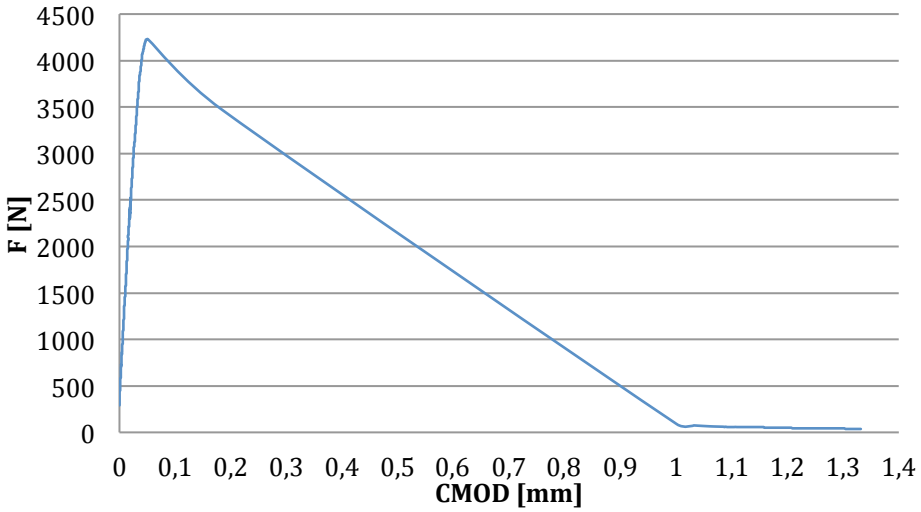

Graph 5-26 - Load vs. CMOD C50_1

5.2.2 C50_2

Another option after testing C50_1 was using a stiffer machine for C50_2. This test took place in the *Structures Lab of UdG* instead of AMADE's lab in the *Parc Tecnològic*. The main difference between both machines is their stiffness, which was not taken into account before. The machine used for C50_2 has a 600 kN capacity (with 100 kN load cell), while in AMADE's lab the machine only has a 100 kN capacity (with 10 kN load cell).

Estimated peak load for the C50_2 specimen was 5500 N, with a 270 N pre-load and a loading block displacement rate of 0,06 mm/min. Values were registered at a frequency of 10 per second.

NOTE1: Very noisy results were obtained. This could be due to the cables of the instrumentation or the load cell capacity being too high. Nevertheless, after taking the average of every 10 values –resulting in one second intervals- the curves were smoother.

NOTE2: Roller supports of D80 mm were used instead of the previously used D20 mm, because those were too small compared to the height of the roller safety stops.

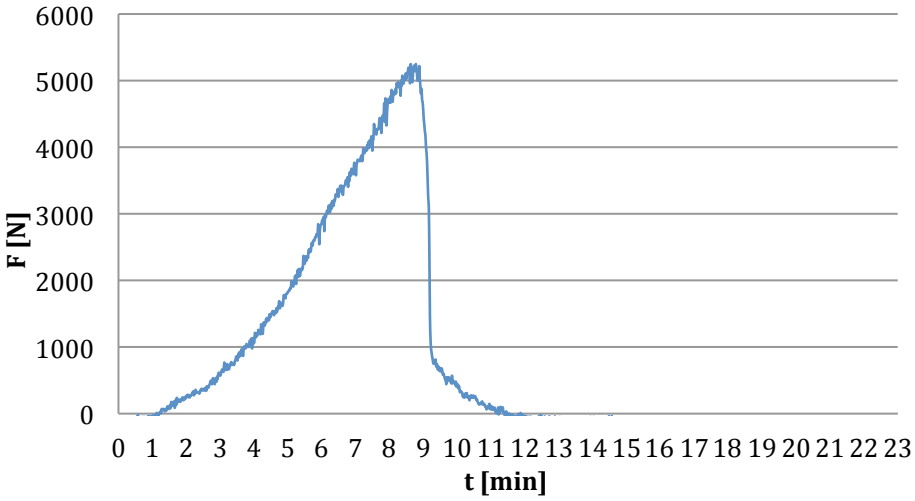

Graph 5-27 - Load vs. time C50_2

Although it seems there is still a sudden crack (sudden load drop), the development of the crack was smoother and resulted in more values in the descending part after the peak load. We may without a doubt conclude that a stiffer machine definitely has an impact on the reaction of the beam to the loading block displacement.

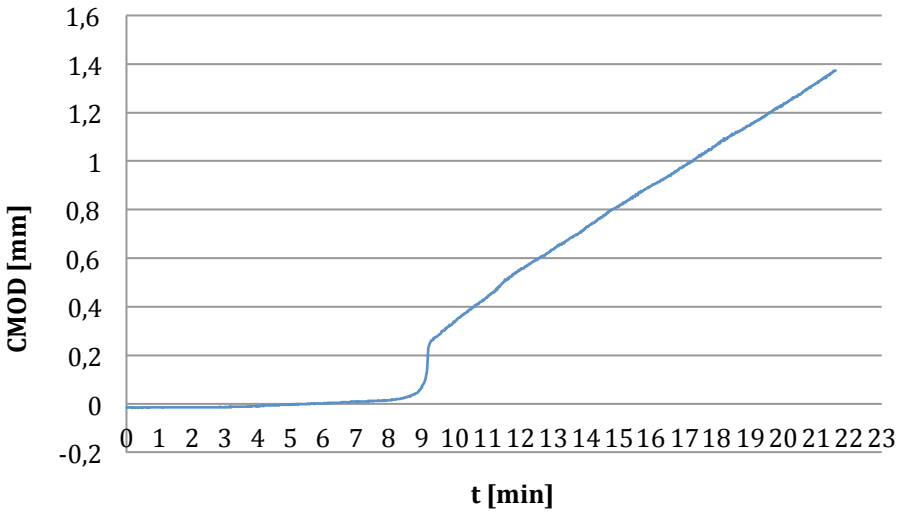

Graph 5-28 - CMOD vs. time C50_2

Compared to the CMOD vs. time for C50_1, this definitely may be considered as an improvement.

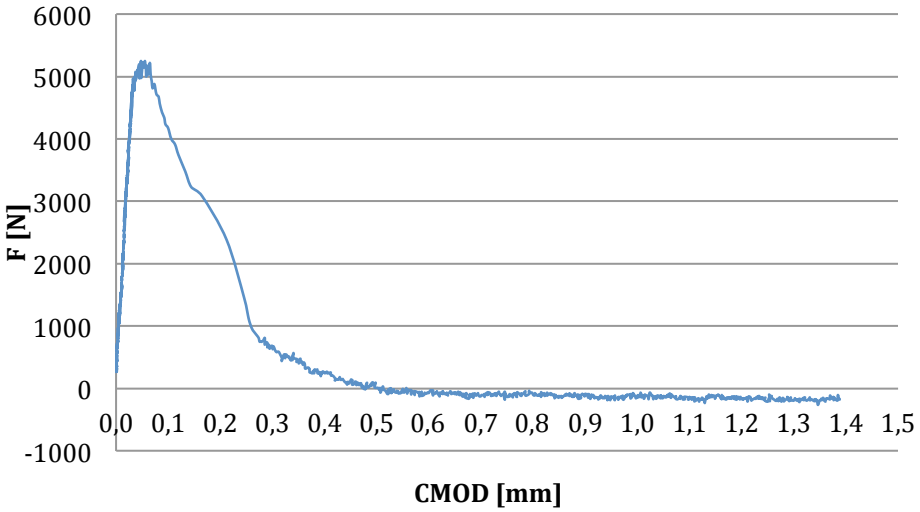

Graph 5-29 – Load vs. CMOD C50_2

The shape of above curve is getting closer to what should be obtained. The unevenness after the peak load is due to the noise of both the load and CMOD registration.

Except for the loading block displacement itself, no external devices were used for load point displacement measurements.

5.2.3 C50_3

An attempt was made to program another machine (*MTS 858 Table Top System 25 kN capacity*) in AMADE with closed-loop CMOD control. The CMOD did not increase enough for the load cell to react. This means that only after the peak load the test with CMOD control would work. If the beam was loaded with constant displacement control until the peak load (most probably with sudden cracking due to limited machine stiffness), and then switched to CMOD control, an important part of data would be missing, namely the parts of the descending curve directly after the peak load. This is why this beam was not further tested, but will be preserved until the program with CMOD control is optimised.

5.2.4 C50_4

The C50_4 specimen will not be tested until a stiffer machine, or one with working closed-loop CMOD control, is available.

5.2.5 Conclusions

The revision of test setup has taught much about the proper conduct of the test. Unfortunately there is not enough time available to find other solutions based on above results and findings. A good base for future tests is formed, and with 2 specimens of the same C50 batch left, future results will easily be comparable. But much more specimens and trials are needed to arrive at a more consistent solution.

6 Determination of modal parameters – bilinear softening curve

The determination of modal parameters such as the initial portion of the cohesive crack model and the bilinear approximation of the entire cohesive crack model, or the (bilinear) softening curve, were not obtained in matters of correct numerical results. This is because the 'load vs. CMOD' curves were not usable due to unstable failure of the beams. However, the calculations have been made in Excel worksheets in collaboration with Xayvanh Oundala, so possible relations between calculation and test results could be made. Since only the trial specimens had stable cracking and thus 'normal' shaped load vs. CMOD curves, these were expected to give acceptable results. The rest of the tests was not analysed due to faulty fracture tests.

Opposed to experimenting with and not worrying about a *correct* method regarding the setup and conduct of the tests, with several other works as guidelines, the details of the calculation method and formulas are beyond the scope of this thesis. Therefore, the ACI 446 report [19] and the improved version of that method [17] (see Appendix C – Detailed data reduction procedure [17]) are followed step-by-step.

6.1 Results

Complete calculations are found from Appendix D – Complete calculation of Trial_C18_1 to Appendix F.

6.1.1 Trial_C18_1

Stress [MPa]	crack width [microns]
1,85	0
0,665082957	55,05115258
0	512,6401395
0	85,95085446 (w_1)

Table 6-1 - Known points for bilinear curve construction Trial_C18_1

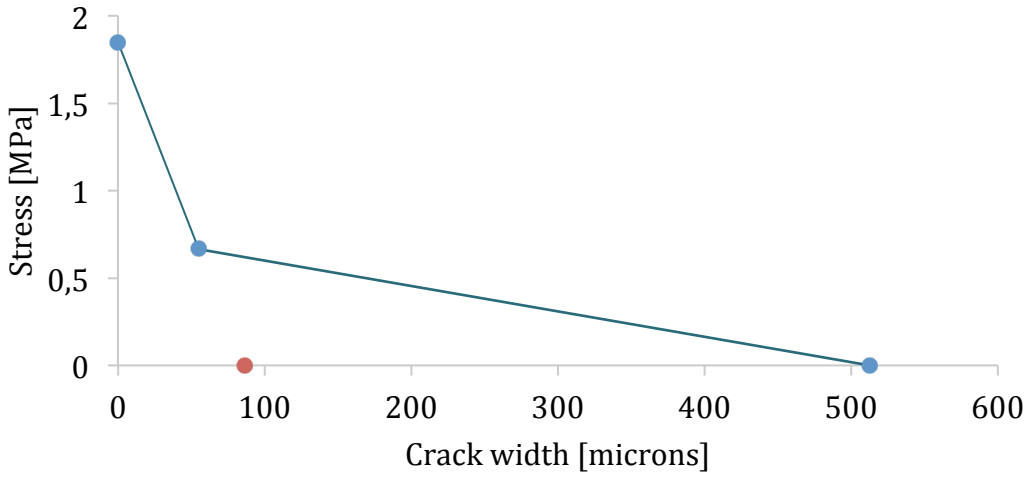

Graph 6-1 - Bilinear approximation of the softening curve Trial_C18_1

One will remark that several calculated values are unlikely to be correct, for example the E-modulus (too low) or the fracture energy G_F (too high) [17]. The CMOD has very important impact on the E-modulus; decreasing the CMOD at the 55% P'max load with 50% for example (from 0,02053 mm to 0,010265 mm; only 0,1mm difference!) increases the E-modulus from 8,4 GPa to 23,5 GPa! Although the shape of the curve looks like it should [8], [28], a high uncertainty regarding the values remains due to limited comparable tests in our case.

6.1.2 Trial_C18_2

Calculations analogue to Trial_C18_1 were made and the shortened results are as follows:

- E = 11,5 GPa
- G_F = 116,5 N/m or J/m^2

Stress [MPa]	crack width [microns]
1,85	0
0,387792368	34,28598898
0	437,3367785
0	43,37898274 (w_1)

Table 6-2 - Known points for bilinear curve construction Trial_C18_2

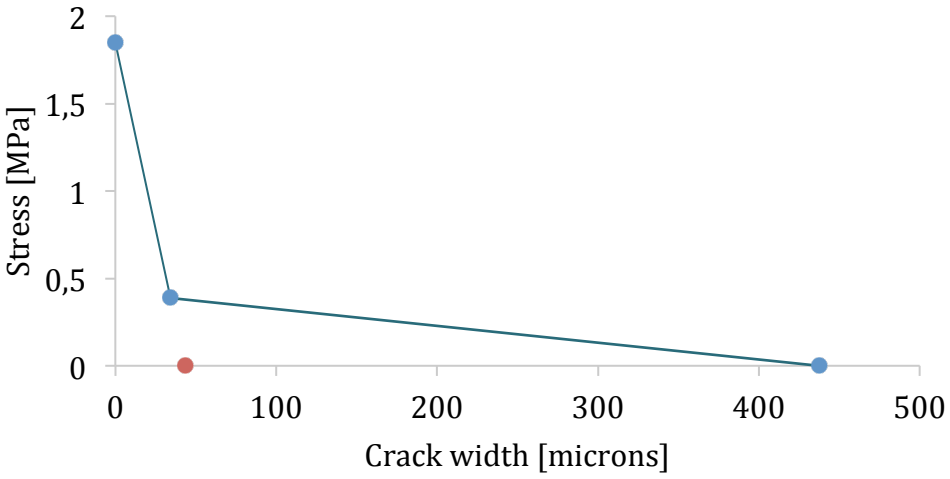

Graph 6-2 - Bilinear approximation of the softening curve Trial_C18_2

The same remarks as for Trial_C18_1 can be made.

6.1.3 C30 specimens

All C30 specimens suffered unstable failure during testing, resulting in incorrect P1 vs. X charts. Therefore it was inutile to try to assess the fracture properties.

6.1.4 C50 specimens

As elaborately discussed in 5.2, only one specimen (C50_2) was somewhat successfully tested. The C50_1 cracked suddenly and the C50_3 test was not completed due to the machine's programming failure.

- E = 68,5 GPa
- G_F = 177,3 N/m or J/m^2

Stress [MPa]	crack width [microns]
3,37	0
2,551283361	3,031612179
0	134,9594107
0	12,47871675 (w_1)

Table 6-3 - Known points for bilinear curve construction C50_2

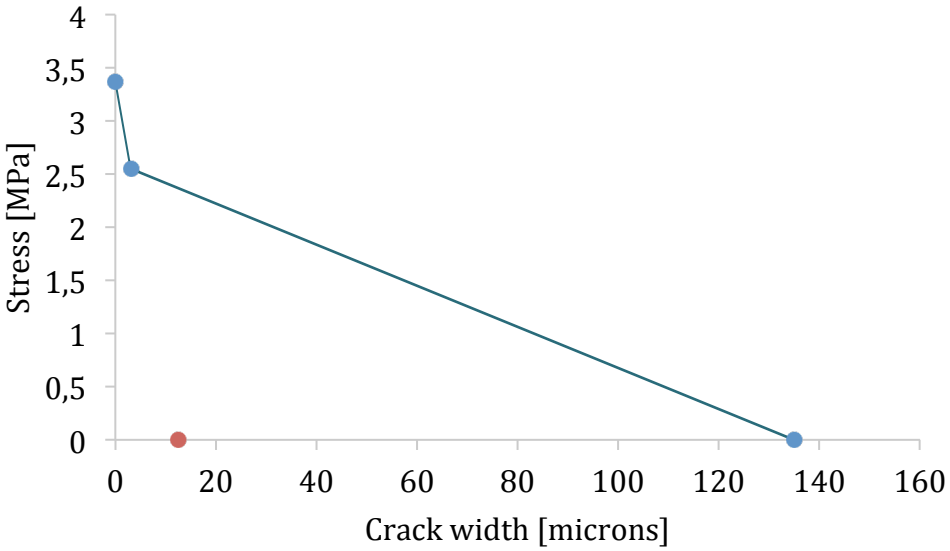

Graph 6-3 - Bilinear approximation of the softening curve C50_2

The value for E is too high this time, but as previously mentioned the CMOD plays a very significant role in this. Since the registered data had a lot of noise, we may assume the calculations for C50 are incorrect. The value for G_F is also still too high. Alas, not enough testing results are available to draw conclusions.

6.2 Conclusion

Although calculations could be made for several specimens, results are fairly useless. Not enough successful, stable tests were performed to achieve consistent and comparable results. It was found that the CMOD measuring preciseness is of remarkably high impact on the E-modulus. Not enough information is known to draw conclusions regarding the fracture energy. More specimens and tests with a stiff enough machine, and eventually CMOD control, are needed to form more consistent conclusions.

7 Conclusions

Although close to no correct (numerical) results were achieved during this thesis, substantial steps forward have been made with respect to the implementation of a fracture test of concrete to determine fracture properties. Mistakes were made, improvements were tried and possible solutions were found. Due to a shortage of time, these probable solutions could not be tried, but we are confident tests with good results are not far away.

Several machines for the three-point bending test have been used, and it was practically confirmed (in one test only, due to time shortage) that the stiffer the machine is, the better the conduct of the test will be. This is most true for the case of when a closed-loop servo control machine setup is unavailable and displacement control has to be performed. The preference to obtain a stable test is of course the usage of a CMOD-control testing machine. Regarding the load point displacement, differences between the reference frame with HLS's and the machine LPD occurred. What should be tried in the future is using the reference frame upside-down, as to have the HLS measure the displacement of the top of the beam instead of the bottom.

Another point that has proven its efficiency is the DIC technique. Even though strains were found to be erroneous, displacements were faultlessly registered. This makes the measurement of the crack mouth opening more accurate because the knives' thickness is not responsible for small deviations anymore. Also the advantages like contactless data registration (no knives to glue!) and millions of data points instead of only one like with analogue measuring devices make the DIC technique interesting to use.

As for the effect of changing concrete parameters, little should have consequences on the conduct of the test itself. The more brittle the concrete is, the higher the chances are that unstable failure will occur, but it should nonetheless be possible to obtain correct load vs. CMOD curves.

This thesis can form a good model for future tests, as several guides and previous research were used and analysed together, as well as several machines (and settings), and various concrete types were used.

8 References

[1] TC89-FMC. (1990b). Size-effect method for determining fracture energy and process zone size of concrete. *Materials and Structures*, *23*(3), 102–106. http://doi.org/10.1007/BF02472030

[2] Bažant, Z., & Planas, J. (1997). *Fracture and size effect in concrete and other quasi brittle material*. CRC Press LLC.

[3] Bažant, Z. P., Yu, Q., & Zi, G. (2002). Choice of standard fracture test for concrete and its statistical evaluation. *International Journal of Fracture*, *118*(4), 303–337. http://doi.org/10.1023/A:1023399125413

[4] Wittman, H. (1987). Fracture toughness and fracture energy of concrete. *International Journal of Cement Composites and Lightweight Concrete*, *9*(4), 252–253. http://doi.org/10.1016/0262-5075(87)90016-9

[5] Hillerborg, A. (1985). The theoretical basis of a method to determine the fracture energy GF of concrete. *Materials and Structures*, *18*(106), 291–296.

[6] Planas, J., & Elices, M. (1989). Material models. *Fracture Mechanics of Concrete Structures*, 16–66.

[7] Bažant, Z. P. (2001). Concrete fracture models: Testing and practice. *Engineering Fracture Mechanics*, *69*(2), 165–205.

[8] Planas, J., Elices, M., Guinea, G. V., Gómez, F. J., Cendón, D. a., & Arbilla, I. (2003). Generalizations and specializations of cohesive crack models. *Engineering Fracture Mechanics*, *70*(14), 1759–1776. http://doi.org/10.1016/S0013-7944(03)00123-1

[9] Pavlovic, M. N. (1996). Fracture mechanics of concrete: applications of fracture mechanics to concrete, rock and other quasi-brittle materials. *Engineering Structures*, *18*(11), 887– 888. http://doi.org/10.1016/0141-0296(96)84816-4

[10] Guo, X. H., Tin-Loi, F., & Li, H. (1999). Determination of quasibrittle fracture law for cohesive crack models. *Cement and Concrete Research*, *29*(7), 1055–1059. http://doi.org/10.1016/S0008-8846(99)00089-7

[11] Guinea, G. V., Planas, J., & Elices, M. (1992). Measurement of the fracture energy using three-point bend tests: Part 1-Influence of experimental procedures. *Materials and Structures*, *25*(4), 212–218. http://doi.org/10.1007/BF02473065

[12] Bornert, M., Brémand, F., Doumalin, P., Dupré, J. C., Fazzini, M., Grédiac, M., ... Wattrisse, B. (2009). Assessment of digital image correlation measurement errors: Methodology and results. *Experimental Mechanics*, *49*(3), 353–370. http://doi.org/10.1007/s11340- 008-9204-7

[13] Pan, B., Xie, H., Wang, Z., Qian, K., & Wang, Z. (2008). Study on subset size selection in digital image correlation for speckle patterns. *Optics Express*, *16*(10), 7037–7048. http://doi.org/10.1364/OE.16.007037

[14] Destrebecq, J. F., Toussaint, E., & Ferrier, E. (2011). Analysis of Cracks and Deformations in a Full Scale Reinforced Concrete Beam Using a Digital Image Correlation Technique. *Experimental Mechanics*, *51*(6), 879–890. http://doi.org/10.1007/s11340-010-9384-9

[15] Yin, Z., Wu, C., & Chen, G. (2014). Concrete crack detection through full-field displacement and curvature measurements by visual mark tracking: A proof-of-concept study. *Structural Health Monitoring*, *13*(2), 205–218. http://doi.org/10.1177/1475921713517289

[16] Pan, B., Qian, K., Xie, H., & Asundi, A. (2009). Two-dimensional digital image correlation for in-plane displacement and strain measurement: a review. *Measurement Science and Technology*.

[17] Fathy, A. M., Sanz, B., Sancho, J. M., & Planas, J. (2008). Determination of the bilinear stress-crack opening curve for normal- and high-strength concrete. *Fatigue and Fracture of Engineering Materials and Structures*, *31*, 539–548. http://doi.org/10.1111/j.1460-2695.2008.01239.x

[18] Massageur, A. (2013). *Guideline for the use of Digital Image Correlation in material and structure characterization tests - 2013-DIC-01* (Vol. 1). Girona.

[19] ACI COMMITTEE 446. (2010). *Fracture toughness testing of concrete*. *Draft ASTM Test Procedure* (Vol. 1).

[20] TC50-FMC. (1985). Determination of the fracture energy of mortar and concrete by means of three-point bend tests on notched beams. *Materials and Structures*, *18*(106), 99–101. http://doi.org/10.1007/BF02472918

[21] TC89-FMC. (1990a). Determination of fracture parameters (K Ic s and CTODc) of plain concrete using three-point bend tests. *Materials and Structures*, *23*(138), 107–110. http://doi.org/10.1007/BF02472029

[22] Shah, S. G., & Kishen, J. M. C. (2011). Fracture Properties of Concrete-Concrete Interfaces Using Digital Image Correlation. *Experimental Mechanics*, *51*(3), 303–313. http://doi.org/10.1007/s11340-010-9358-y

[23] Yaofeng, S., & Pang, J. H. L. (2007). Study of optimal subset size in digital image correlation of speckle pattern images. *Optics and Lasers in Engineering*, *45*(9), 967–974. http://doi.org/10.1016/j.optlaseng.2007.01.012

[24] Beygi, M. H. a, Kazemi, M. T., Nikbin, I. M., & Amiri, J. V. (2013). The effect of water to cement ratio on fracture parameters and brittleness of self-compacting concrete. *Materials and Design*, *50*, 267–276. http://doi.org/10.1016/j.matdes.2013.02.018

[25] Yi, S.-T., Kim, J.-K., & Oh, T.-K. (2003). Effect of strength and age on the stress–strain curves of concrete specimens. *Cement and Concrete Research*, *33*(8), 1235–1244. http://doi.org/10.1016/S0008-8846(03)00044-9

[26] Barris, C., Vilanova, I., Torres, L., Mias, C., Massaguer, A. (2014). Analysis of cracking of GFRP RC beams with a digital image correlation system. In *Proceedings of the 7th International Conference on FRP Composites in Civil Engineering*. Vancouver, Canada.

[27] Mazzoleni, P. (2013). Uncertainty estimation and reduction in digital image correlation measurements. In *Doctoral Dissertation*.

[28] Guinea, G. V., Planas, J., & Elices, M. (1994). A general bilinear fit for the softening curve of concrete. *Materials and Structures*, *27*(2), 99–105. http://doi.org/10.1007/BF02472827

APPENDIX

A – Reference frame

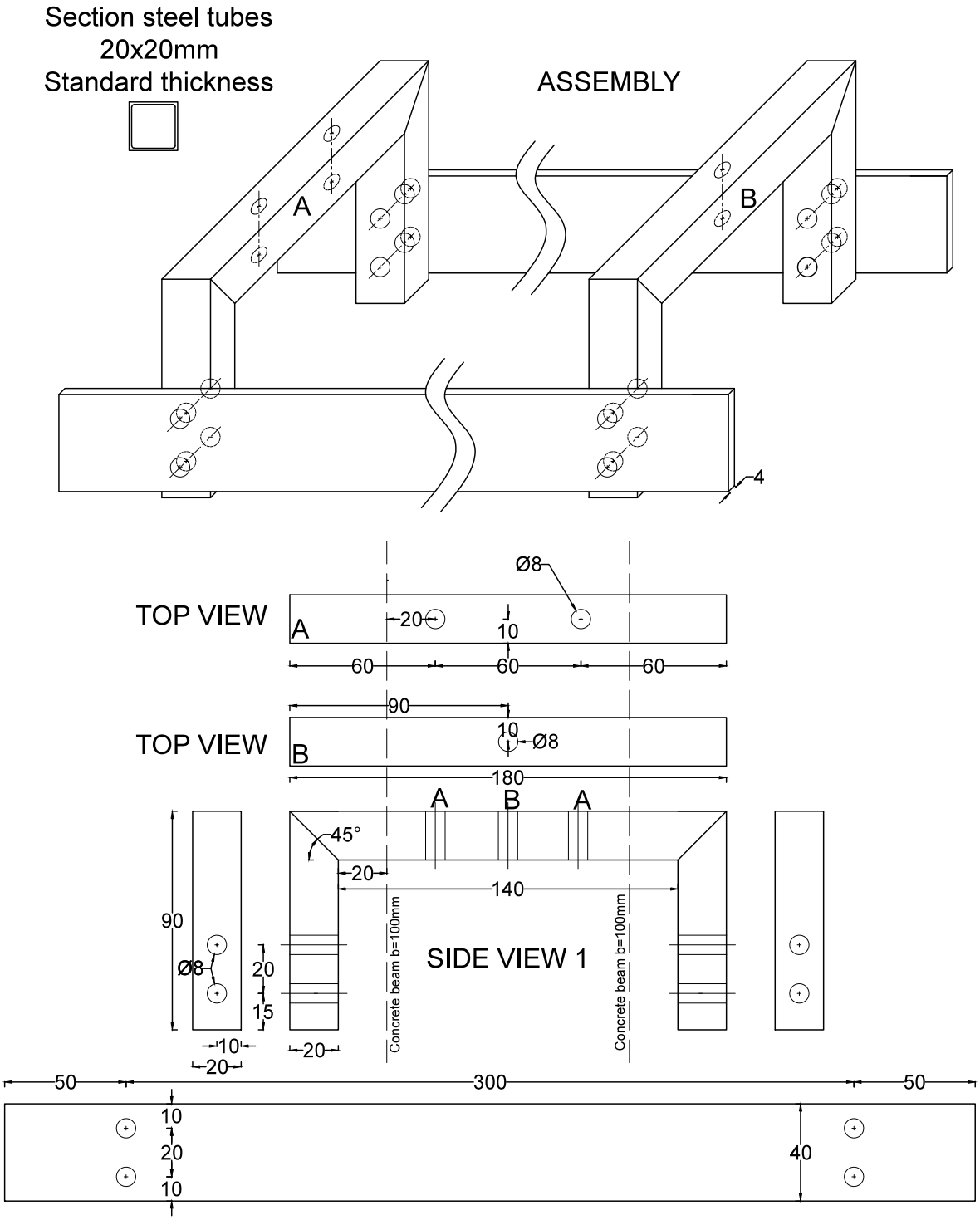

NOTE: Some adjustments were made during manufacturing:

• Bolt diameter 6 was used instead of 8mm; the 45° welds were executed horizontally; minor distance adaptations

B – MATLAB average code

```
clear all;
clc;

%% Import original rows from Excel file
FILE = 'C30_1_input.xlsx'; %change filename
[NUM,TXT,RAW]=xlsread(FILE);
r=30676;  %this is the number of values (= dividable by 'n') +1
Array_1 = cell2mat(RAW(2:r,1)); %(from row:to row, column)
Array_2 = cell2mat(RAW(2:r,2));
Array_3 = cell2mat(RAW(2:r,3));
Array_4 = cell2mat(RAW(2:r,4));
Array_5 = cell2mat(RAW(2:r,5));
Array_6 = cell2mat(RAW(2:r,6));

%% Choose filter length
n = 50;       % filter length

a1 = reshape(Array_1,n,[]);
a2 = reshape(Array_2,n,[]);
%a3 = reshape(Array_3,n,[]); %unnecessary columns when HLS not registered
%a4 = reshape(Array_4,n,[]);
a5 = reshape(Array_5,n,[]);
a6 = reshape(Array_6,n,[]);

b1 = sum(a1,1)./size(a1,1);
b2 = sum(a2,1)./size(a2,1);
b5 = sum(a5,1)./size(a5,1);
b6 = sum(a6,1)./size(a6,1);

%% Export new arrays to Excel as COLUMNS (transpose)

%filename='C30_1_avg.xlsx'; %REMARK1: export to Excel impossible on Mac

tb1 = b1';
tb2 = b2';
tb3 = tb2*0;      %add these columns to the excel file but as 0-columns
tb4 = tb2*0;      when HLS is not registered
tb5 = b5'*-1;     %make the displacement positive
tb6 = b6'*-1;     %make the load positive

M = [tb1,tb2,tb3,tb4,tb5,tb6];

%sheet = 8;                     %REMARK1
%xlRange = 'A1';
%xlRange2 = 'B1';
%xlswrite(filename,tryy,sheet,xlRange);
%xlswrite(filename,trbb,sheet,xlRange2);

dlmwrite('C30_1_avg05.txt',M);  %REMARK1: write to .txt instead
```

C – Detailed data reduction procedure [17]

1.1 *Compute the average tensile strength f_{tm} from the splitting tensile strength test as:*

a. Determine the tensile strength f_t for each specimen:

$$f_t = \frac{2P_u}{\pi DL}$$

where: f_t = tensile strength, MPa

P_u = ultimate load, N

D = specimen diameter, mm

L = specimen length, mm

b. Compute f_{tm} as the mean of every f_t value.

1.2 *Elastic modulus, E:*

a. On the raising branch of the P'-CMOD curve, select the test points where measured load P' lies between 15% and 55% of the measured peak load.

b. Fit a straight line to this segment then use a linear regression of the P'-CMOD to identify the slope of the segment. It is taken as an initial compliance of the specimen:

$$C_i = \frac{\Delta CMOD}{\Delta P'}$$

where: C_i = initial compliance, $\mu m\ N^{-1}$

$\Delta CMOD$ = variation of CMOD, μm.

$\Delta P'$ = variation of measured load, N.

c. Determine the elastic modulus for each specimen:

$$E = \frac{6Sa_0V_1(\alpha_0')}{C_iBD^2}, \text{ with } \alpha_0' = \frac{(a_0+h)}{(D+h)}$$

where: E = elastic modulus, GPa.
B = beam thickness, mm.
D = beam depth, mm.
a_0 = notch length, mm.
h = thickness of the steel knife, mm.

$$V_1(\alpha) = 0.8 - 1.7\alpha + 2.4\alpha^2 + \frac{0.66}{(1-\alpha)^2} + \frac{4D}{S}(-0.04 - 0.58\alpha + 1.47\alpha^2 - 2.04\alpha^3)$$

1.3 *Far tail constant, A:*

a. From the recoded data, remove all the points with CMOD > 4D/300.

b. Observe the values of the load and the CMOD at the last point of the curve, call them P_R' and w_{MR} respectively.

C' – Detailed data reduction procedure [17] (2)

c. Compute the corrected load for every point in the record as:

$$P_1 = P' - P_1'$$

d. Plot the graph with P_1 versus CMOD then determine w_{MA} which is the CMOD value for zero load on the rising raising branch.

e. Calculate the auxiliary values for points that have smaller value than 5% of corrected peak load ($P_1 < 0.05P_{1u}$) in the tail parts of the graph.

$$X = (4D/S)^2[1/(w_M - w_{MA})^2 - 1/(w_{MR} - w_{MA})^2]$$

f. Plot the values of P_1 against X then fit the curve with the equation

$$P_1 = X(A + KX)$$

1.4 *The net plastic flexural strength, f_p :*

a. Determine the effective maximum load:

$$P_u = P_{1u} + A/(w_{MR} - w_{MA})^2$$

where: P_u = effective peak load, N.
P_{1u}=maximum corrected peak load, N.

b. Calculate the net plastic flexural strength for each specimen as:

$$f_p = P_u S/[2B(D - a_0)^2]$$

where: f_p = net plastic flexural strength, MPa.

1.5 *Fracture energy, G_F:*

a. Plot the corrected peak load P_1 versus mid-span deflection δ for each test. Identify δ_A, deflection corresponds to zero load on the loading part and δ_R on the unloading part.

b. Compute the measured fracture work as the area enclosed by the curve $P_1 - \delta$ and the δ axis.

c. The total work of fracture is taken as:

$$W_F = (W_{Fm} + 2A)/(\delta_R - \delta_A)$$

where: W_F=total work of fracture, Nmm (mJ).

W_{Fm}= measured work of fracture, Nmm (mJ).

d. Compute the fracture energy after the following expression:

$$G_F = 1000W_F/[B(D - a_0)]$$

where: G_F=fracture energy, N/m (J/m^2).

C" – Detailed data reduction procedure [17] (3)

1.6 *Centre of gravity of the softening curve, w_G:*

a. For each specimen, determine the centre of gravity as:

$$w_G = (4A \times 10^6)/BSG_F$$

where: w_G=centre of gravity of the area under the softening curve, μm (microns).

1.7 *Determine the parameters of the bilinear approximation of the softening curve:*

a. The brittleness length, compute for each specimen:

$$l_1 = (1 - \alpha_0^{1.7})D\left[\frac{11.2}{(x^2-1)^2} + \frac{2.365}{x^2}\right]$$

where: l_1= brittleness length, mm.

$\alpha_0 = a_0/D$=notch-to-depth ratio.

x=f_{tm}/f_p=inverse relative plastic strength.

b. The horizontal intercept of the bilinear curve is calculated as:

$$w_1 = 1000 \times 2 f_{tm} l_{1m}/E_m$$

where: w_1=horizontal intercept, μm (microns).

E_m =mean elastic modulus, MPa.

c. The characteristic crack opening defined as:

$$w_{ch} = G_{Fm}/f_{tm}$$

where: w_{ch}= characteristic crack opening, μm (microns).

d. Compute the critical crack opening of the bilinear approximation as:

$$w_c = w_{ch}\frac{3w_{Gm}-w_1}{2w_{ch}-w_1} \times \left[+\sqrt{1 - \frac{2w_1(3w_{Gm}-2w_{ch})(2w_{ch}-w_1)}{w_{ch}(3w_{Gm}-w_1)^2}}\right]$$

where: w_c=critical crack opening, μm (microns).

e. Determine the coordinates (σ_k, w_k) of the kink point of the bilinear curve:

$$\sigma_k = f_{tm}\frac{2w_{ch} - w_1}{w_c - w_1}$$

where: σ_k=stress at the kink point, MPa.

and $w_k = w_1\frac{w_c-2w_{ch}}{w_c-w_1}$

where: w_k=crack opening at the kink point, μm (microns).

D – Complete calculation of Trial_C18_I

Bilinear approximation

Beam depth, D	100	mm
Beam thickness, B	100	mm
Length, L	600	mm
Span, S	300	mm
Notch length, a_0	33,33	mm
Compression strength	18,5	MPa
Tensile strength	1,85	MPa
Thickness of the two steel knives, h	2	mm

I. Determine the mean elastic modulus, E

Recorded peak load, P'max	3013,9	N		
15% P'max	452,085	N	corresponding CMODs	0,00458 mm
55% P'max	1657,645	N		0,02053 mm
Initial compliance Ci	0,01323036	µm/N		
α_0'	0,34637254	mm		
$V_1(\alpha)$	1,84486634			
Elastic modulus	8,36567271	GPa		

II. Determine the far tail constant A

4D/300 = w_{MR}	1,33333333	mm
P'_R	269,49	N
w_{MA}	0,00243	mm
Maximum corrected load, P_{1u}	2744,41	N
0.05 P_{1u}	137,2205	N
Plot P1 vs. X chart		
A-term	248,950	N

III. Compute the net plastic flexural strength, fp

The effective maximum load, P_u	2885,027	N
f_p	0,97359912	MPa

D' – Complete calculation of Trial_C18_I (2)

IV. The mean fracture energy, G_F

δ_A	0,047	mm
δ_R	1,099	mm
W_{Fm}	1002,761	Nmm(mJ)
W_F	1476,04997	Nmm(mJ)
G_F	221,396426	N/m(J/m^2)

V. The centre gravity of softening curve w_G

w_G	149,927141	µm

VI. Brittleness length, l_1

l_1	194,334248	mm

VII. The horizontal intercept of the softening curve, w_1

w_1	85,9508544	µm

VIII. The characteristic crack opening, w_{ch}

w_{ch}	119,673743	µm

IX. The critical length of the bilinear approximation, w_c

1st term of the equation	283,845646	
2nd term of the equation	1,80605250	
w_c	512,640139	µm

X. Compute the coordinate of the bilinear kink point curve, σ_k and w_k

σ_k	0,66508295	MPa
w_k	55,0511525	µm

E – Complete calculation of Trial_C18_2

Bilinear approximation

Beam depth, D	100	mm
Beam thickness, B	100	mm
Length, L	600	mm
Span, S	300	mm
Notch length, a_0	50	mm
Compression strength	18,5	MPa
Tensile strength	1,85	MPa
Thickness of the two steel knives, h	2	mm

I. Determine the mean elastic modulus, E

Recorded peak load, P'max	1668,23	N		
15% P'max	250,2345	N	corresponding CMODs	0,00458 mm
55% P'max	917,5265	N		0,02053 mm
Initial compliance Ci	0,02355490	µm/N		
α_0'	0,50980392	mm		
$V_1(\alpha)$	3,00517708			
Elastic modulus	11,4823613	GPa		

II. Determine the far tail constant A

4D/300 = w_{MR}	1,33333333	mm
P'_R	163,705	N
w_{MA}	0,0009813	mm
Maximum corrected load, P_{1u}	1504,528	N
0.05 P_{1u}	75,2264	N
Plot P1 vs. X chart		
A-term	102,700	N

III. Compute the net plastic flexural strength, fp

The effective maximum load, P_u	1562,537	N
f_p	0,93752216	MPa

E' – Complete calculation of Trial_C18_2 (2)

IV. The mean fracture energy, G_F

δ_A	0,002300	mm
δ_R	1,017000	mm
W_{Fm}	380,138000	Nmm(mJ)
W_F	582,562362	Nmm(mJ)
G_F	116,512472	N/m(J/m^2)

V. The centre gravity of softening curve w_G

w_G	117,526760	µm

VI. Brittleness length, l_1

l_1	134,619772	mm

VII. The horizontal intercept of the softening curve, w_1

w_1	43,378983	µm

VIII. The characteristic crack opening, w_{ch}

w_{ch}	62,979715	µm

IX. The critical length of the bilinear approximation, w_c

1st term of the equation	235,811384	
2nd term of the equation	1,854604	
w_c	437,336779	µm

X. Compute the coordinate of the bilinear kink point curve, σ_k and w_k

σ_k	0,387792	MPa
w_k	34,285989	µm

F – Complete calculation of C50_2

Bilinear approximation

Beam depth, D	100	mm
Beam thickness, B	100	mm
Length, L	600	mm
Span, S	300	mm
Notch length, a_0	31	mm
Compression strength	58,6	MPa
Tensile strength	3,37	MPa
Thickness of the two steel knives, h	2	mm

I. Determine the mean elastic modulus, E

Recorded peak load, P'max	5248,6	N		
15% P'max	787,29	N	corresponding CMODs	0 mm
55% P'max	2886,73	N		0,003 mm
Initial compliance Ci	0,00142895	µm/N		
α_0'	0,32352941	mm		
$V_1(\alpha)$	1,75299507			
Elastic modulus	68,4537284	GPa		

II. Determine the far tail constant A

4D/300 = w_{MR}	1,33333333	mm
P'_R	215,56	N
w_{MA}	0	mm
Maximum corrected load, P_{1u}	5033,04	N
0.05 P_{1u}	251,652	N
Plot P1 vs. X chart		
A-term	59,430	N

III. Compute the net plastic flexural strength, fp

The effective maximum load, P_u	5066,608	N
f_p	1,59628493	MPa

F' – Complete calculation of C50_2 (2)

IV. The mean fracture energy, GF

δ_A	0,9	mm
δ_R	1,3	mm
W_{Fm}	926	Nmm(mJ)
W_F	1223,15	Nmm(mJ)
G_F	177,268115	N/m(J/m^2)

V. The centre gravity of softening curve w_G

w_G	44,7006499	µm

VI. Brittleness length, l_1

l_1	52,6018148	mm

VII. The horizontal intercept of the softening curve, w_1

w_1	12,4787167	µm

VIII. The characteristic crack opening, w_{ch}

w_{ch}	52,6018148	µm

IX. The critical length of the bilinear approximation, w_c

1st term of the equation	68,9955114	
2nd term of the equation	1,9560607	
w_c	134,95941	µm

X. Compute the coordinate of the bilinear kink point curve, σ_k and w_k

σ_k	2,5512833	MPa
w_k	3,0316121	µm

FACULTEIT INDUSTRIELE INGENIEURSWETENSCHAPPEN
TECHNOLOGIECAMPUS GENT
Gebroeders De Smetstraat 1
9000 GENT, België
tel. + 32 9 265 86 10
fax + 32 9 225 62 69
iiw.kaho.gent@kuleuven.be
www.iiw.kuleuven.be